4 Theranostic chitosan nanoparticles for the co-delivery of PLB and UMN

4.1 Objective of the study

Theranostic nanoparticles have gained significant attention in cancer diagnosis and therapy. The objective of the study was to develop estrone (ES) and folic acid (FA) functionalized single and dual receptor targeted theranostic chitosan nanoparticles for breast cancer imaging and therapy. These nanoparticles (NPs) were loaded with palbociclib (PLB) and ultra-small magnesium nanoclusters (UMN). Developed theranostics NPs were characterized for physicochemical properties, *in vitro* characterization and *in vivo* evaluation.

4.2 Plan of the study

- Preparation of PLB and UMN loaded dual receptor targeted theranostic NPs using solvent evaporation combined with an ionic cross-linking method.
- Physicochemical and in-vitro evaluation of dual receptor targeted theranostic NPs
- Particle size, polydispersity index, and zeta potential by DLS
- Electron microscopy (SEM, TEM & AFM)
- Crystallographic studies by XRD
- Surface chemistry by XPS
- Determination of entrapment efficiency
- *In vitro* drug release studies
- *In vitro* cellular uptake study on MCF-7 and T-47D cells
- *In vitro* cytotoxicity study on MCF-7 and T-47D cells
- *In vitro* cell cycle study on MCF-7 cells
- *In vivo* pharmacokinetic and histopathology studies in SD rats
- *In vivo* optical, ultrasound/photoacoustic imaging

- Anticancer efficacy studies on DMBA induced breast tumor rat model, tumor targeting efficiency and survival analysis.

4.3 Materials

Sun Pharmaceutical Industries Limited, Gurugram, India, provided complimentary palbociclib (PLB) samples. Chitosan (CS) with a molecular weight of approximately 1.5 kDa and a degree of deacetylation greater than 90%, as well as Estrone (ES), Folic acid (FA), succinic anhydride (SA), Sodium-tripolyphosphate (Na-TPP), 4-(Dimethylamino)pyridine (DMAP), N-Hydroxysuccinimide (NHS), triethylamine (TEA), and N-(3-dimethylaminopropyl)-N-ethylcarbidiimide (EDC), were sourced from SRL, India. Magnesium chloride was supplied by Merck India. Estrone succinate (ES-COOH) [137], chitosan-estrone (CS-ES) [138] and chitosan-folate (CS-FA) [109] were prepared by previously reported methods. MCF-7 and T-47D human breast cell lines were acquired from NCCS Pune, India. Genetix Biotech Asia Pvt. Ltd, supplied chemicals and nutrients for cell works. Eppendorf provided 96-well plates and T-25 cell culture flasks. All other chemicals used in the research were of analytical grade.

4.4 Methods

4.4.1 Preparation of UMN

Ultra-small magnesium nanocluster (UMN) as an imaging agent was prepared as per the method reported by Srivastava et al [139]. UMN as an imaging agent was prepared using the reported method. Briefly, all the glassware was cleansed with aqua regia (HCl(3): HNO_3 (1)) and then rinsed two to three times with distilled water and ethanol. $MgCl_2$ salt solution (10 mM, 10 mL) and BSA solution (450 mg/mL, 1 mL) were used to synthesize BSA-templated magnesium nanoclusters. L-ascorbic acid (35 mg/mL, 3 mL) was added after mixing both solutions for 5 min (55°C, 900 rpm). The solution was then maintained for 2 h at 55° C with constant vigorous agitation. After 2 h of reaction, the colorless solution became pale yellow. The solution was then incubated for 15 h at 55° C. The color of the

solution changed from light to pale yellow, indicating the completion of the reaction. The nanoclusters were centrifuged (15,000 rpm for 10 min) to remove larger particles. Further, UMN suspension was freeze dried and stored at 4°C. The prepared UMN was characterized for fluorescent intensity and transmission electron microscopy.

4.4.2 Formulation of theranostic NPs

Theranostic NPs were developed by using UMN as an imaging agent and PLB as a therapeutic agent. The co-loading of both components in the CS-NPs was achieved by modified emulsion solvent evaporation followed by an ionic crosslinking technique [140]. In brief, a solution of the 30 mg chitosan was prepared in 0.2 % v/v of the acetic acid, and 2 mg of the UMN was transferred to it and vortexed to get a homogeneous solution. The solution pH 6.0 was adjusted by using dil. NaOH and added 20 mg of the TPGS (surfactant). Separately, 3 mg of the PLB was dissolved in 1 mL of chloroform. Both polymeric solution and drug solution were mixed, and the emulsion was prepared using an ultrasonic probe sonicator (Hielscher UP200H, Germany). The formed emulsion was magnetically stirred for 4 h. After evaporation of the chloroform, a dropwise addition of 1 mL of sodium TPP (1 mg/mL) solution was added for ionic crosslinking of NPs suspension. The developed NPs were subjected to centrifugation at 3000 rpm for 10 min to remove larger NPs. Additionally, after separation of the larger NPs, desired NPs were collected from the NPs suspension by centrifugation at 14000 rpm for 10 min. The obtained pellets were washed with distilled water and suspended in phosphate buffer saline (pH 7.4). **Table 4.1.** displays the composition of the different theranostic NPs formulations.

For the targeted delivery of the NPs, they were prepared as per the above mentioned methods, with the replacement of 10 mg of CS with 10 mg CS-ES (for ER targeting), 10 mg of CS-FA (for folate receptor targeting), and 10 of each CS-ES and CS-FA (for dual receptor targeting).

The formulation of chitosan NPs using sodium TPP involves a complex process that leverages the interaction between the positively charged amino groups of chitosan and the negatively charged phosphate groups of sodium TPP. A spontaneous electrostatic interaction between chitosan and sodium TPP leads to the formation of polyelectrolyte complexes. These complexes act as crosslinks between chitosan chains, resulting in the formation of NPs. Sodium TPP serves as a crosslinking agent, facilitating the formation of a three-dimensional network within the chitosan solution. As the crosslinking progresses, the NPs stabilize due to the electrostatic interactions and physical entanglement between the chitosan chains and sodium TPP molecules. Since chitosan was preconjugated with ES or FA, targeting moiety will be assembled on the surface of targeted NPs.

Table 4.1 The formulation composition of the FR targeted, nontargeted, ER targeted, and dual receptor targeted theranostic NPs

Formulations	CS (mg)	TPGS (mg)	CS-ES (mg)	CS-FA (mg)	PLB (mg)	UMN (mg)	Sod. TPP (mg)
Blank CS NPs	30	20	-	-	-	-	1
PLB-UMN-CS-NPs	30	20	-	-	3	2	1
PLB-UMN-CS-ES-NPs	20	20	10	-	3	2	1
PLB-UMN-CS-FA-NPs	20	20	-	10	3	2	1
PLB-UMN-CS-ES-FA-NPs	10	20	10	10	3	2	1

Blank CS NPs: Blank chitosan NPs
PLB-UMN-CS-NPs: Nontargeted theranostic NPs
PLB-UMN-CS-ES-NPs: Estrogen receptor targeted theranostic NPs
PLB-UMN-CS-FA-NPs: Folate receptor targeted theranostic NPs
PLB-UMN-CS-ES-FA-NPs: Estrogen and folate receptor targeted theranostic NPs

4.4.3 Characterization of nanoparticles

4.4.3.1 Particle size, zeta potential, and polydispersity index

The developed NPs were subjected to analysis by using a Zetasizer (Nano ZS90, Malvern Instruments) to obtain the average particle size and zeta potential. The values presented are the means of three measurements [105].

4.4.3.2 Entrapment efficiency

The entrapment efficiency (% EE) of PLB within the nanoformulations were analyzed by utilizing the reverse phase validated HPLC (SIMADZU LC-20AR, Japan) method [106]. In order to rupture the NPs, 200 µL of the NPs dispersion was dried and then mixed with 1 mL of methanol, and bath sonication was done for 1 h. Upon an appropriate dilution in the mobile phase, it passed through a 0.22 µm nylon filter and was then subjected to HPLC analysis. The standard calibration curve for PLB exhibited linearity with an R^2 value of 0.998, covering a concentration range of 10 to 60 ng/mL. To quantify PLB, we employed a validated HPLC analytical method. This method utilized a mobile phase composed of acetonitrile (30%) and methanol (70%). The HPLC parameters were a flow rate of 1 mL/min, an injection volume of 100 µl, a retention time of 4.8 min, and a PDA detector with a maximum wavelength set at 355 nm (λmax). The HPLC system had a Shimadzu Shim-pack C18 column, which played a critical role in separating and quantifying PLB.

The amount of UMN entrapped in the chitosan NPs was determined using an indirect method involving a multimode microplate reader in fluorescent mode. After completing the sample preparation process, measurements were carried out in fluorescence mode with an excitation wavelength of 469 nm and an emission wavelength of 543 nm. The resulting standard curve showed linearity within the 10-100 µg/mL concentration range, with an R^2 value of 0.999. % EE of PLB or UMN were determined by the following formulae:

$$Entrapment\ efficiency\ (\%) = \frac{Amount\ of\ the\ drug\ or\ UMN\ entrapped\ in\ the\ NPs}{Amoun\ of\ the\ drug\ or\ UMN\ used\ in\ the\ NPs\ preparation} * 100$$

4.4.3.3 High resolution scanning electron microscopy (HR-SEM)

Morphology of the prepared PLB-UMN-CS-NPs, PLB-UMN-CS-FA-NPs, PLB-UMN-CS-ES-NPs, and PLB-UMN-CS-FA-ES-NPs were obtained by HR-SEM (Nova

Nano SEM 450, FEI USA). The PLB-UMN-CS-NPs, PLB-UMN-CS-FA-NPs, PLB-UMN-CS-ES-NPs and PLB-UMN-CS-FA-ES-NPs suspensions were diluted tenfold with purified water, NPs suspension were placed onto a coverslip separately, ensuring even distribution. The coverslip was then placed in a vacuum drier overnight. Once the dried thin films were prepared, a layer of carbon was applied to them, and microscopic photographs were taken by HR-SEM [107].

4.4.3.4 Transmission electron microscopy (TEM)

PLB-UMN-CS-NPs, PLB-UMN-CS-FA-NPs, PLB-UMN-CS-ES-NPs and PLB-UMN-CS-FA-ES-NPs images were taken by utilizing TEM (FEI Tecnai G2 F20 X-TWIN). The suspensions of nanoformulations were tenfold diluted in purified water before being deposited onto a separate TEM grid with a 400-mesh. The TEM grid, with the dried NPs cast on it, was then subjected to vacuum drying. Subsequently, TEM was used to capture images of the samples [108].

4.4.3.5 Atomic force microscopy (AFM)

Furthermore, using AFM (NTEGRA Prima, Netherlands), pictures of the NPs in two and three dimensions were taken. Following a tenfold dilution with purified water, a droplet of the NPs samples was cast onto individual glass slides and evenly spread to create thin films. Additionally, samples cast as films underwent low-pressure vacuum drying in a vacuum drier. The images were then taken and analyzed using AFM image analysis software (Nova Px from NT-MDT, Netherlands). [109].

4.4.3.6 Surface analysis by XPS

Surface elemental composition of the PLB-UMN-CS-NPs, PLB-UMN-CS-FA-NPs, PLB-UMN-CS-ES-NPs, and PLB-UMN-CS-FA-ES-NPs were analyzed by X-ray photoelectron spectroscopy (XPS, K-Alpha, Thermo Fisher Scientific Inc A dried thin film of the NPs was scanned for 10-800 eV of binding energy to detect C, N, O and Mg content

in the samples [110]. The % amount of the targeting moiety present on the NPs surface were determined based on their elemental composition.

4.4.3.7 ES/FA surface content

PLB-UMN-CS-ES-NPs PLB-UMN-CS-ES-NPs and PLB-UMN-CS-FA-ES-NPs were processed for the calculation of their ES content on the NPs surface was performed by using a multimode microplate reader. Briefly, 0.3 mL of NPs were dried and then mixed with a solution of DMSO to DCM in a 4:1 ratio. After 4 h of vortexing and subsequent centrifugation, the processed samples supernatant was filtered through a 0.22 µm filter and subjected to analysis at 296 nm [111]. The amount of ES present in the PLB-UMN-CS-ES-NPs and PLB-UMN-CS-FA-ES-NPs was determined by the given formula.

$$ES\ \ content\ (\%)\ = \frac{ES\ content\ determined\ in\ the\ nanoparticles}{Total\ ES\ content\ unsed\ in\ the\ nanoparticles} * 100$$

Similarly, for determining FA content in the PLB-UMN-CS-FA-NPs and PLB-UMN-CS-FA-ES-NPs, samples were processed as per the above method and the absorbance of the sample was recorded at 364 nm. The % FA content was estimated by using the following method [141].

$$FA\ \ content\ (\%) = \frac{Folate\ content\ determined\ within\ NPs}{Total\ folate\ content\ used\ in\ NPs} * 100$$

4.4.3.8 X-ray diffraction study (XRD)

The pure drug, excipients, and lyophilized NPs were scanned by Rigaku MiniFlex X-ray diffractometer in the range of 5-80° (2θ) by applying a voltage of 40kV with a 5°/min scan rate. The XRD analysis will be helpful in the identification of the physical state of drug distribution within the NPs [142].

4.4.4 *In vitro* studies

4.4.4.1 *In vitro* drug release

The dialysis bag diffusion techniques were used for the *in vitro* release of PLB from NPs. The NPs suspension containing 300 µg of the PLB was kept inside the dialysis bag (1000 Da) and sealed on both ends. Further, an *in vitro* release study was carried out at 37±0.5°C in a beaker containing 100 mL of PBS 7.4 pH. The sealed dialysis tube was immersed, and continuous shaking of the setup was maintained at 100 rpm. At each predetermined sampling time point, 1 mL of the sample was withdrawn and replaced with 1 mL of fresh buffer. Additionally, free PLB was also tested for *in vitro* release. Similarly, free drug and developed NPs *in vitro* drug release were evaluated at pH 6.5 PBS and pH 4.5 acetate buffer. Samples were diluted, filtered and collected in HPLC vials for analysis by using a validated RP-HPLC analytical method [143].

4.4.4.2 Evaluation of hemocompatibility of NPs

The evaluation of biocompatibility between the NPs and blood was carried out to assess their impact on red blood cells. A 10 mL blood sample was taken in a heparinized tube. Red blood cells (RBCs) were then isolated after centrifuging at 3000 rpm. The RBC that settled at the bottom of the tube underwent 2-3 washes with a normal saline solution before being suspended in the same solution. Additionally, 0.9 mL of RBCs suspension and 0.1 mL of different NPs (i.e., PLB, PLB-UMN-CS-NPs, PLB-UMN-CS-FA-NPs, PLB-UMN-CS-ES-NPs and PLB-UMN-CS-FA-ES-NPs) were incubated together. RBC suspensions in distilled water served as the positive control, while RBC suspensions in saline were used as the negative control. These samples were kept at 37°C with gentle shaking for 1 h. When RBCs take up water and subsequently swell and burst, distilled water causes 100% hemolysis. Following the incubation period, smears were prepared, and

Leishman stain was applied to individual glass slides with a drop of the specimens. After staining, a bright microscope was employed to capture images of the stained RBCs. Furthermore, the incubated specimens underwent a 5 min centrifugation at 3000 rpm. The supernatants from these samples were collected, and their UV absorbance at 540 nm was measured utilizing a microplate reader. As per the ASTM E2524-22 standard, test materials below 5% of hemolysis are safer, whereas if hemolysis exceeds 5%, then test materials are hemolytic in nature and not suitable for *i.v.* administration [113].

$$\%\ Hemolysis = \frac{Abs\ Test - Abs\ negative\ control}{Abs\ Positive\ control - Abs\ negative\ control} * 100$$

4.4.4.3 *In vitro* physiological stability

The *in vitro* physiological stability of the developed NPs was evaluated in the plasma and serum of female rats. Briefly, equal volumes of the NPs suspension and plasma or serum were incubated at 37°C for 24 h, separately. Following incubation, NPs were collected and evaluated for particle size, zeta potential, and entrapment efficiency.

4.4.4.4 Maintenance of the cell lines

Dulbecco's Modified Eagle Medium (DMEM) supplemented with 10% Fetal Bovine Serum (FBS) and the antibiotic solution Penicillin-Streptomycin was employed for the culture of T-47D and MCF-7 breast cancer cells. Throughout the study, a 5% CO_2 environment was maintained, and the T-47D and MCF-7 cells were cultured in a humidified CO_2 incubator.

4.4.4.5 Confocal laser scanning microscopy (Cellular uptake)

The cellular internalization process of developed NPs, including free UMN, PLB-UMN-CS-NPs, PLB-UMN-CS-FA-NPs, PLB-UMN-CS-ES-NPs, and PLB-UMN-CS-FA-ES-NPs, were examined in the MCF-7 and T-47D cell lines using confocal microscopy (Wetzlar, Germany). Initially, a population of 1×10^5 MCF-7 and T-47D cells was cultured

for 24 h on a coverslip placed within a 6-well cell culture plate, separately. Subsequently, the cells were treated with individual samples containing free UMN, PLB-UMN-CS-NPs, PLB-UMN-CS-FA-NPs, PLB-UMN-CS-ES-NPs, and PLB-UMN-CS-FA-ES-NPs, each at a concentration of 20 µg/mL (with respect to UMN), for 2 h. Following this incubation, the cells underwent two rounds of cold phosphate-buffered saline (PBS) washing. After the incubation period, the cells were fixed using a 4% paraformaldehyde solution and then subjected to three additional washes with cold phosphate-buffered saline (PBS). To visualize the fixed cells nuclei, they were stained with propidium iodide (PI) during a 30-minute incubation. In experiments involving receptor blocking to study cellular uptake, the cells were pretreated with free ES and FA at a concentration of 2 mg/mL for 6 h. This pretreatment was followed by treatment with PLB-UMN-CS-FA-ES-NPs. The cellular monolayers were visualized using confocal microscopy [114].

4.4.4.6 Cytotoxicity assay

The free PLB, PLB-UMN-CS-NPs, PLB-UMN-CS-FA-NPs, PLB-UMN-CS-ES-NPs and PLB-UMN-CS-FA-ES-NPs cytotoxicity assay were performed in ER and FR overexpressed T-47D and MCF-7 cells. In brief, DMEM-seeded cells were cultured at a density of 1 x 10^4 cells per well for 12 h at 37°C in a CO_2 humidified incubator with 5% CO_2. After this 12 h incubation period, the used medium was discarded, and the cells were incubated with various concentrations of free PLB, PLB-UMN-CS-NPs, PLB-UMN-CS-FA-NPs, PLB-UMN-CS-ES-NPs, and PLB-UMN-CS-FA-ES-NPs (0.01 µg/mL, 0.1 µg/mL, 1 µg/mL, 10 µg/mL, 100 µg/mL), all diluted in DMEM medium. The cells were then cultured for an additional 24 h. A volume of 100 µL of media containing MTT (5 mg/mL in PBS, pH 7.4) was added to each well of the plate after the removal of the drug containing media. The plate was subsequently incubated for 2 h. The formazan crystals were not disturbed during this process, and the crystals were subsequently rinsed and dried

for an additional 2 h. Following 2 h of washing and drying period, 100 µL of DMSO was added to each well. The optical densities of the samples were then measured at 570 nm using a microplate reader (BioRad Multiplate reader) [114]. The determination of cellular viability was carried out utilizing the given formula.:

$$\%\ Cellular\ viability\ = \frac{Absorbance\ of\ the\ treated\ cells}{Absorbance\ of\ the\ control\ cells} * 100$$

4.4.4.7 Cell cycle analysis

A study was conducted to analyze the cell cycle of developed nanoformulations, including free PLB, PLB-UMN-CS-NPs, PLB-UMN-CS-FA-NPs, PLB-UMN-CS-ES-NPs, and PLB-UMN-CS-FA-ES-NPs, in MCF-7 cell lines [116]. In brief, 1 x 10^5 MCF-7 cells were cultured in 6-well plates using complete DMEM and allowed to adhere for 24 h in a CO_2 incubator. Subsequently, the MCF-7 cells were individually incubated with free PLB, PLB-UMN-CS-NPs, PLB-UMN-CS-FA-NPs, PLB-UMN-CS-ES-NPs, and PLB-UMN-CS-FA-NPs. Following the treatment, the cells were collected using a chilled PBS containing 1 mM EDTA. The cells were fixed with 70% ethyl alcohol and then incubated at -20 °C for 12 h. Subsequently, the cells were treated with a PI-RNAse solution containing 1 mg/mL PI, 0.1% V/V Triton X-100, and 10 mg/mL RNAse, and they were maintained at 37 °C for 30 min before being rinsed with chilled PBS. The cell cycle analysis was performed using a flow cytometer (CytoFLEX, Beckman Coulter, USA).

4.4.5 *In vivo* studies

4.4.5.1 Pharmacokinetic study

The study involved female Sprague Dawley (SD) rats weighing 150-200 g and aged 40-60 days. These rats were sourced from the animal house of the Institute of Medical Science BHU, India. Ethical approval for the animal experiments was obtained from the Institutional Animal Ethics Committee (IAEC) at IIT BHU, India (IAEC Approval Number: IIT(BHU)/IAEC/2022/047). Each group in the study consisted of three rats.

Before commencing the experimental procedures, the rats were housed in a controlled environmental setting with a consistent room temperature. The rats had unrestricted access to water and were provided with standard rat food. They underwent a one-week acclimatization period during which they were exposed to a natural light/dark cycle.

The rats were divided into five groups, each comprising three individuals (n=3). In Group I, rats received intravenous (*i.v.*) injections of pure PLB suspended in phosphate buffer saline. Group II rats were given with PLB-UMN-CS-NPs. Group III was given with PLB-UMN-CS-FA-NPs. Group IV rats were given PLB-UMN-CS-ES-NPs. Finally, Group V rats underwent treatment with PLB-UMN-CS-FA-ES-NPs [143]. Before I.V. injections, all NPs underwent filtration using a 0.45 µm syringe filter. Following filtration, terminal sterilization was conducted by exposing the NPs to UV light for a duration of 2 h. The administration of various nanoformulations was performed via *i.v.* injection (5.91 mg/kg of body weight). After the injection of the nanoformulations, a volume of 400 µl of rat blood was transferred into EDTA containing tubes. Blood samples were collected at specified time points: 0.5, 1, 2, 4, 8, 12, 24, and 48 h. The plasma from each blood sample was isolated through centrifugation at 5000 rpm for 5 min at a temperature of 4°C. An equivalent amount of acetonitrile was introduced to the plasma samples to remove plasma proteins, causing protein precipitation. The samples then underwent centrifugation at 15000 rpm for 15 min to eliminate the precipitated proteins. The collected plasma samples were quantified for the amount of the PLB by using HPLC.

4.4.5.2 Histopathology Study

Histopathological analysis was employed to assess the safety and toxicity of the developed nanoformulations after repeated dosing in rats (n=3). The groups included vehicle control (saline), drug control (free PLB), folate receptor-targeted NPs (PLB-UMN-CS-FA-NPs), ER-targeted NPs (PLB-UMN-CS-ES-NPs), and dual-targeted NPs (PLB-

UMN-CS-FAES-NPs). These nanoformulations were administered intravenously at doses of 5.91 mg/kg (equivalent to PLB), with three days between each dose. On the fifteenth day, all groups of animals were euthanized, and their vital organs were carefully excised and washed with PBS before being mounted in a cryostat. Tissue specimens were then sliced into sections with a thickness of 5 μm using a Leica CM1950 cryomicrotome. Subsequently, the sections were stained with hematoxylin and eosin (H & E) dye for histological examination. The pictures of all specimens were collected by using a light microscope [117]. Pictures of all specimens were collected using a light microscope.

4.4.5.3 Animals

Female SD rats, with a weight of approximately 200 g and an age range of 60-70 days, were housed in a standard environment at ambient temperature and provided with a standard diet. The Institutional Animal Ethics Committee (IAEC) at the Indian Institute of Technology (Banaras Hindu University), Varanasi, India, approved all *in vivo* animal experiments (IAEC Approval Number: IIT(BHU)/IAEC/2022/047) and all experiments were conducted in accordance with the National Research Council's Guide for the Care and Use of Laboratory Animals.

4.4.5.4 Tumor induction

Breast tumors in the SD rats were induced by using 7,12-dimethylbenz(a)anthracene (DMBA) at a dose of 25 mg/kg body weight. DMBA was dissolved in the almond oil and injected subcutaneously into the rat’s breast pad (left or right). At the beginning of the 8-week DMBA administration period, all rats were assessed for the development of tumors. The mammary pad was palpated regularly during the screening process to detect the presence of any suspicious masses. After approximately 75 days of DMBA administration, the tumor size became stable [118-120]. The rats were regularly palpitated once the tumor diameter became above 6 mm and were chosen for the

in vivo experiments. Reports have demonstrated that DMBA induced SD rats were found to have overexpressed ER and PR [121]. Additionally, a cell line extracted from DMBA-induced breast cancers displays characteristics that are similar to those of the MCF-7 cell line [122].

4.4.5.5 Grading of breast tumor

Breast tumors developed in rats after administration of DMBA were removed and cleaned with PLBS. A 5 µm thick section was prepared from the tumor paraffin block using a microtome. The globally accepted standard method for distinguishing tumors from healthy tissue is Hematoxylin and Eosin (H & E) staining. In accordance with established procedures, an H & E stain was applied to the obtained tumor section. Healthy rat breast was also extracted and stained with H&E to compare with the breast tumor.

4.4.5.6 *In vivo* breast tumor imaging by USG/PA

The *in vivo* anticancer investigation was conducted on female SD rats with induced breast tumors. Six groups, each consisting of three rats with breast tumors, were randomly assigned for the study. Before receiving NPs therapy, all rats with breast tumors underwent ultrasound and photoacoustic (USG/PA) imaging system scans using a 40-MHz ultrasound array transducer (Vevo LAZR_X, Toronto, Canada) [144, 145]. Various imaging modes were employed to examine the mammary tumors. Each animal received an equivalent dose of 5.91 mg/kg of PLB, either the free drug or NPs. Group I, serves as disease control (no drug treatment). In Group II, rats received *i.v.* injections of pure PLB suspended in sterilized phosphate buffer saline. Group III rats were injected with PLB-UMN-CS-NPs. Group IV was injected with PLB-UMN-CS-FA-NPs. Group V rats were given PLB-UMN-CS-ES-NPs. Finally, Group VI rats underwent treatment with PLB-UMN-CS-FA-ES-NPs. Imaging at 0 days refers to imaging of rats prior to administration of free drugs or formulations. After 2, 4, and 6 days following the treatments, USG/PA imaging of the rats

was performed. Image processing was performed by the Vevo LAB software for each dataset [146].

4.4.5.7 *In vivo* fluorescent imaging of the breast tumor

The targeted delivery of the theranostic NPs to the breast cancer bearing rat after *i.v.* administration of the developed theranostic NPs and free UMN was investigated by using the Photon IMAGER-Optima system (Biospace Lab). The *in vivo* fluorescence produced after administration of the free UMN (control) and PLB-UMN-CS-NPs, PLB-UMN-CS-FA-NPs, PLB-UMN-CS-ES-NPs, and PLB-UMN-CS-FA-ES-NPs to the SD rats with breast tumor at an equivalent dose of 200 µg of UMN. Fluorescent data were collected at 469 nm excitation and 543 nm emission wavelengths at four different time points: 0.5, 2, 4, and 6 h after injection. The obtained images were processed by using M3Vision software, and the ROI of circled breast tumors was calculated [110].

4.4.6 Statistical analysis

All the data of studies were demonstrated as a mean of three repetitive measurements with standard deviation. All the obtained data were statistically calculated by using GraphPad Prism 7.0. Statistical significance between groups was assessed using the one-way ANOVA and post-Tukey test. The following values were used to determine the statistical significance level: ns ($P \geq 0.05$), * ($P < 0.05$), ** ($P < 0.01$), *** ($P < 0.001$), and **** ($P < 0.0001$).

4.5 Results and discussion

4.5.1 Characterization of UMN

Fluorescence spectra of the prepared UMN were collected by using a spectroflurophotometer. UMN suspension in water was subjected to the fluorescence scan, and images were captured. **Figure 4.1.A**. demonstrates the blue (excitation, 366 nm) and green (excitation, 469 nm) fluorescence of UMN. TEM analysis demonstrated the ultrasmall and uniform size of the UMN (**Figure 4.1B**). Additionally, UMN aqueous

suspension depicted 366 nm and 469 nm excitation spectra with 451 nm and 543 nm emission spectra, respectively (**Figure 4.1C and 1D**). Hence, the developed UMN can be used as an imaging agent for *in vitro* and *in vivo* experiments.

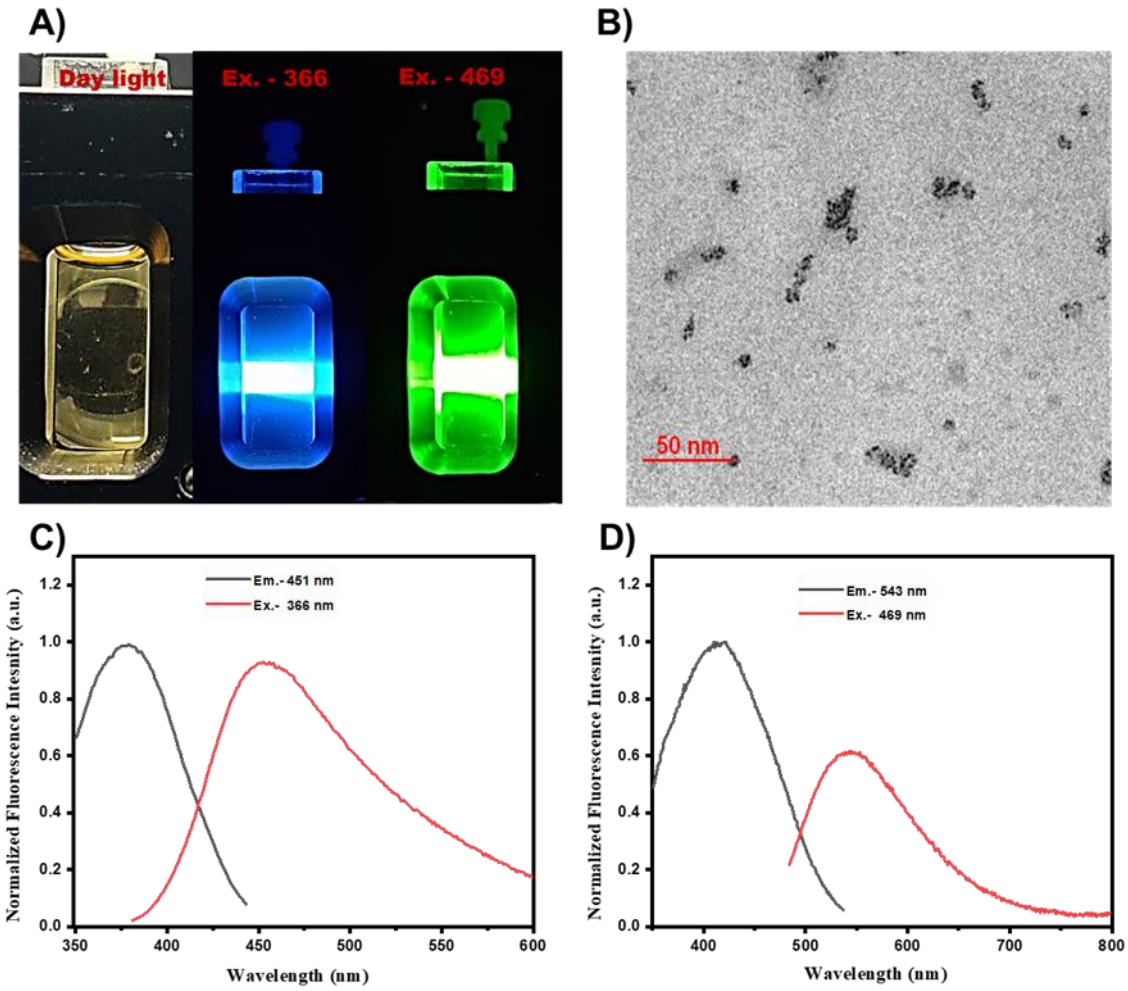

Figure 4.1 A) Fluorescent images of UMN at day light, Ex 366 nm (blue) and Ex 469 nm (green), B) TEM image of UMN, C) and D) UMN excitation and emission spectra.

4.5.2 Nanoparticles characterization

4.5.2.1 Particle size, zeta potential, and polydispersity index

The physicochemical evaluation of the developed nanoformulation has been presented in **table 4.2**. The results demonstrated that prepared NPs had particle size in the range of 150.1 ± 1.83 nm to 198.2 ± 1.43 nm. The obtained data suggested that all NPs were below 200 nm. It was noted that blank CS-NPs had 150.1 nm and +20.62 mV particle size and zeta potential, respectively. The incorporation of PLB inside NPs enhanced the particle size

(178.4 nm) with little lowering in zeta potential (+19.02 mV). Additionally, in the case of FR targeted NPs and ER targeted NPs, incorporation of the CS-FA and CS-ES has significantly improved the particle size (185.1 nm and 181.6 nm) with lowered zeta potential (+16.72 mV and +13.89 mV), respectively. Additionally, dual-targeted NPs had 198.2 nm particle size and +15.23 mV zeta potential. The presence of ES and/or FA on the nanoformulation surfaces contributed to the increase in size. In contrast, the reduction of free NH_2 in targeted NPs primarily accounted for the decrease in zeta potential.

Table 4.2. Particle size, polydispersity, zeta potential, entrapment efficiency, and IC_{50} value of developed NPs.

Batches	PS (nm) (mean ± S.D*)	PDI (mean ± S.D*)	ZP (mV) (mean ± S.D*)	EE (mean ± S.D*)	IC_{50} (µg/ml) (mean ± S.D*)	
				PLB	MCF-7	T-47D
PLB	-	-	-	-	40.63±1.94	48.15±1.85
Blank CS-NPs	150.1 ± 1.83	0.210±0.048	+20.62± 0.318	-	-	-
PLB-UMN-CS-NPs	178.4 ± 1.21	0.230±0.042	+19.02± 0.382	74.15 ± 1.83	4.15±0.38	5.92±0.83
PLB-UMN-CS-ES-NPs	181.6± 1.35	0.191±0.031	+13.89±0.410	76.82± 1.84	1.29±0.05	1.65±0.06
PLB-UMN-CS-FA-NPs	185.1± 1.33	0.212±0.014	+16.72± 0.527	75.92± 2.01	1.56±0.04	2.07±0.09
PLB-UMN-CS-ES-FA NPs	198.2± 1.43	0.198±0.021	+15.23±0.377	73.04± 1.98	0.75±0.08	1.14±0.03

*n = 3; S.D: Standard deviation
PLB-UMN-CS-NPs: Nontargeted theranostic NPs
PLB-UMN-CS-ES-NPs: Estrogen receptor targeted theranostic NPs
PLB-UMN-CS-FA-NPs: Folate receptor targeted theranostic NPs
PLB-UMN-CS-ES-FA-NPs: Estrogen receptor and folate receptor targeted theranostic NPs

4.5.2.2 Entrapment efficiency evaluation

The amount of PLB loaded in PLB-UMN-CS-NPs, PLB-UMN-CS-FA-NPs, PLB-UMN-CS-ES-NPs and PLB-UMN-CS-FA-ES-NPs were determined to be 74.15 ± 1.832 %, 75.92± 2.014 %, 76.82 ± 1.847 % and 73.04 ± 1.982 %, respectively **(Table 4.2)**. The entrapment of PLB was not affected much by the incorporation of the CS-ES and/or CS-FA during the formulation of the targeted nanoformulation. Additionally, the amount of UMN entrapped in the PLB-UMN-CS-NPs, PLB-UMN-CS-FA-NPs, PLB-UMN-CS-ES-

NPs and PLB-UMN-CS-FA-ES-NPs were found to be 58.24±1.08 %, 61.02±0.94 %, 57.31±1.07 % and 59.14±1.17 %, respectively.

4.5.2.3 FE-SEM

The surface morphological images of the developed nanoformulation were taken by FE-SEM and presented in **figure 4.2A**. The microscopic images of the NPs depicted that developed formulations had round morphology with smooth surfaces. Additionally, from the images, it can also be confirmed that developed NPs had uniform particle size distribution [124].

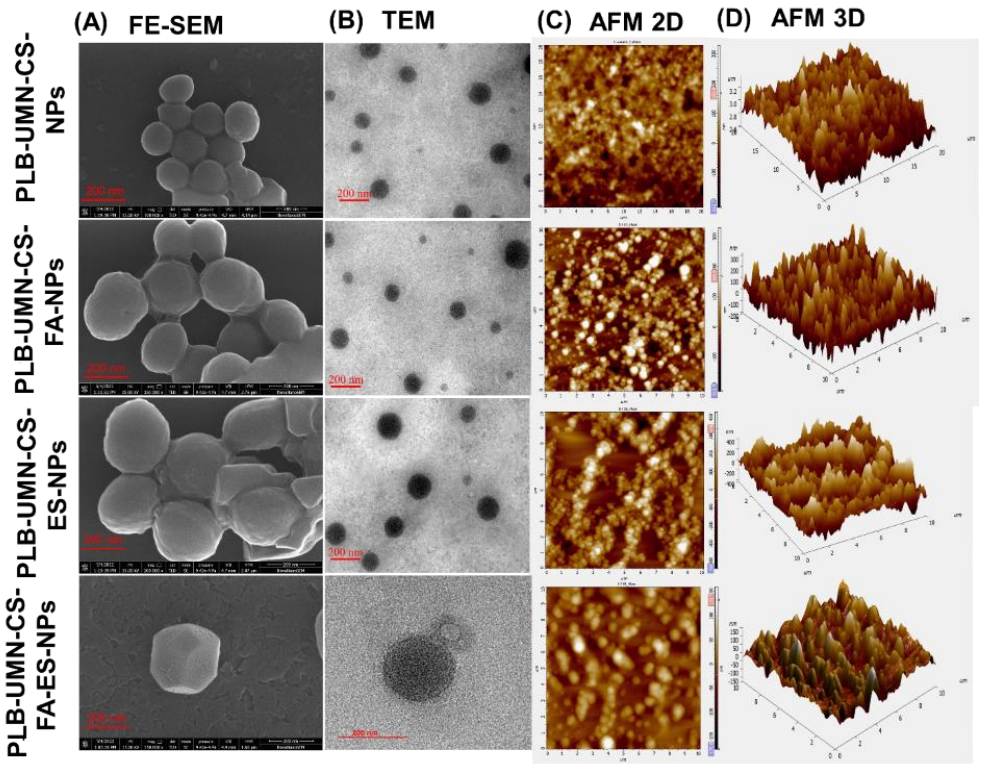

Figure 4.2 Microscopic images of PLB-UMN-CS-NPs, PLB-UMN-CS-FA-NPs, PLB-UMN-CS-ES-NPs, and PLB-UMN-CS-FA-ES-NPs by (A) FE-SEM, (B) TEM, (C) 2D AFM) and (D) 3D AFM.

4.5.2.4 TEM

The images of the developed NPs were captured using an electron beam with TEM. These techniques provide higher resolution photographs. TEM images of NPs at a scale of

200 nm are presented in **Figure. 4.2B**. Developed NPs appeared to exhibit a perfectly round shape in the images.

4.5.2.5 AFM

The topography of the NPs in both two and three dimensions was examined using AFM. This technique yields high-quality images of the NPs without relying on optical methods. The two dimensional and three dimensional images of AFM, presented in **figure 4.2 C** and **D** revealed that all developed NPs were uniformly distributed and had round morphology.

4.5.2.6 Surface chemistry by XPS

The NPs surface elemental composition was determined by using XPS. The developed NPs such as PLB-UMN-CS-NPs, PLB-UMN-CS-FA-NPs, PLB-UMN-CS-ES-NPs, and PLB-UMN-CS-FA-ES-NPs surface elemental composition of C1s, N1s and O1s were examined and presented in the **figure 4.3A**. The percentage of C1s, N1s and O1s in the PLB-UMN-CS-NPs was observed to be 68.55 %, 2.82 % and 28.62 %, respectively, whereas PLB-UMN-CS-FA-NPs, depicted of C1s, N1s and O1s as 68.64 %, 3.59 % and 27.77 %, respectively. PLB-UMN-CS-ES-NPs demonstrated C1s, N1s and O1s signal with 73.71 %, 1.54 % and 24.75 %, respectively and PLB-UMN-CS-FA-ES-NPs depicted C1s, N1s and O1s signal with an intensity of 71.07 %, 3.11 % and 25.75%, respectively. The reduction % of nitrogen in the PLB-UMN-CS-ES-NPs can be attributed to the prior conjugation of nitrogen atoms in the CS with ES. As a result, the nitrogen atoms on the surface of the PLB-UMN-CS-ES-NPs were observed to be less abundant compared to the PLB-UMN-CS-NPs.

4.5.2.7 ES/FA surface content

The amount of the ES on PLB-UMN-CS-ES-NPs and PLB-UMN-CS-FA-ES-NPs surfaces were 78.10 ± 1.6 % and 74.85 ± 1.3 %, respectively. Similarly, the amount of the

FA on PLB-UMN-CS-FA-NPs and PLB-UMN-CS-FA-ES-NPs surfaces were 73.24 ± 1.7 % and 71 ± 2.4 %, respectively.

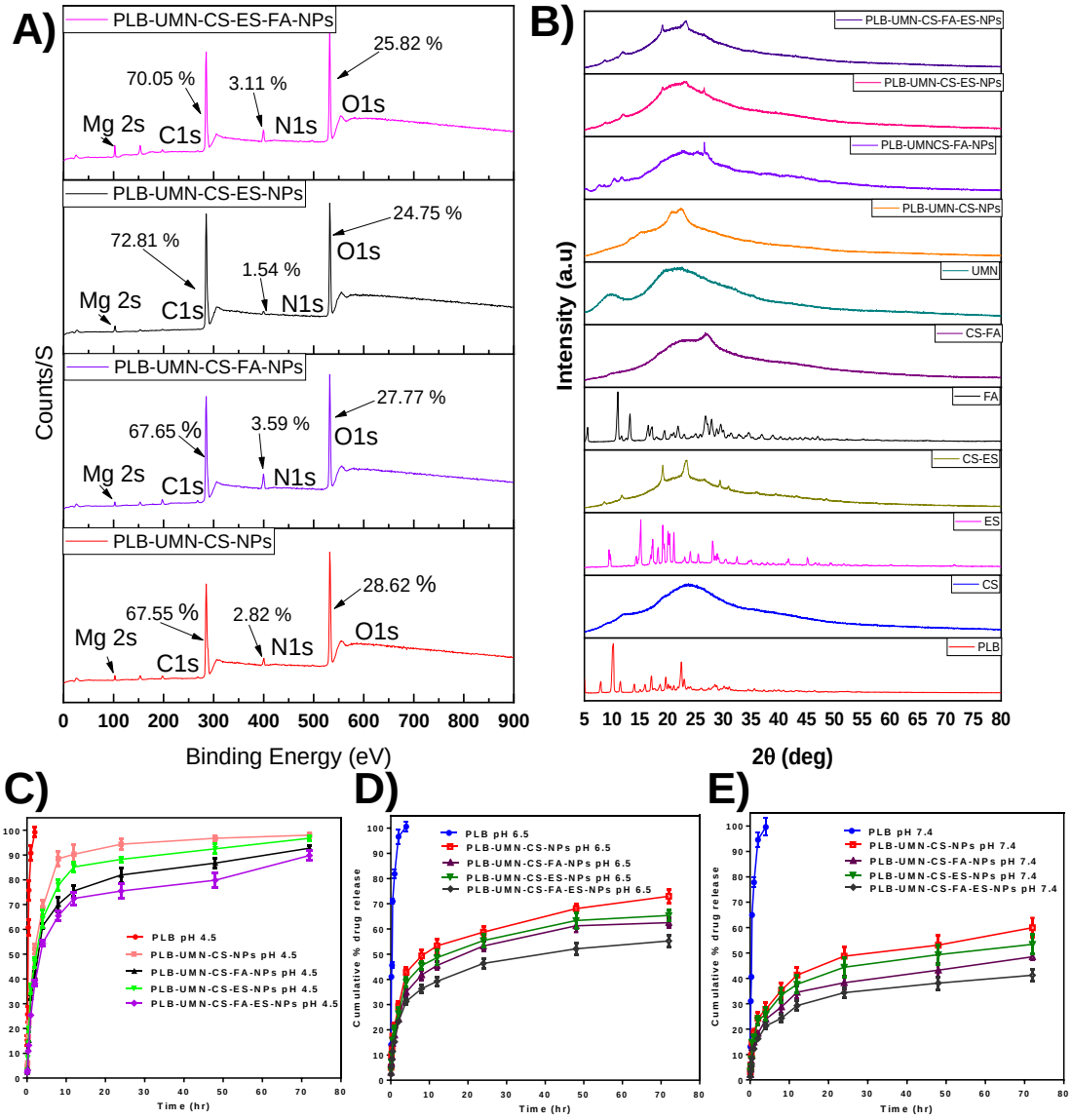

Figure 4.3 A) XPS analysis of PLB-UMN-CS-NPs, PLB-UMN-CS-FA-NPs, PLB-UMN-CS-ES-NPs and PLB-UMN-CS-FA-ES-NPs by XPS, B) XRD graph of PLB, CS, ES, FA, UMN, CS-ES, CS-FA, PLB-UMN-CS-NPs, PLB-UMN-CS-FA-NPs, PLB-UMN-CS-ES-NPs and PLB-UMN-CS-FA-ES-NPs. *In vitro* PLB release at C) pH 4.5, D) pH 6.5, and E) pH 7.4 from nanoformulations.

4.5.2.8 XRD Study

An XRD investigation enabled the assessment of drug phase identification in its nanoformulation. XRD analysis is a common technique used to track any changes in the physical structure of a drug that may occur during the development of a nanoformulation.

Most therapeutic agents exist in either a crystalline or amorphous state. In contrast to its crystalline state, the amorphous state offers improved solubility and enhanced bioavailability [147]. XRD measurements of PLB revealed multiple distinct and well-defined diffraction peaks at 2θ=7.92°, 10.14°, 11.52°, 13.94°, 15.96°, 16.95°,18.60°,19.68, 22.40°, and 22.68°. **Figure 4.3B** indicates that pure PLB can be observed in its crystalline state, confirming alignment with recently published findings [126]. In PLB-UMN-CS-NPs, PLB-UMN-CS-FA-NPs, PLB-UMN-CS-ES-NPs, and PLB-UMN-CS-FA-ES-NPs, all of the PLB peaks were absent, indicating that the drug had transitioned into an amorphous state due to the NPs formulations. This suggests that the resulting nanoformulation incorporated PLB at the molecular level. Since the amorphous form of the drug is more bioavailable than its crystalline form, the prepared NPs may increase the bioavailability of PLB. Additionally, it was observed that crystalline nature of the ES and FA has been reduced after conjugation of CS.

4.5.3 *In vitro* studies

4.5.3.1 *In vitro* drug release studies

PLB release profile from PLB-UMN-CS-NPs, PLB-UMN-CS-FA-NPs, PLB-UMN-CS-ES-NPs and PLB-UMN-CS-FA-ES-NPs at 7.4 pH, 6.5 pH and 4.5 pH have been demonstrated in **figure 4.3C-3E**. For simulating the physiological pH of a human, which is 7.4, an *in vitro* release study was performed. Additionally, the tumor microenvironment has a slightly acidic pH. In order to simulate tumor microenvironment, *in vitro* release was performed at pH 4.5 and 6.5 [128, 148].

The drug release pattern from PLB-UMN-CS-NPs, PLB-UMN-CS-FA-NPs, PLB-UMN-CS-ES-NPs, and PLB-UMN-CS-FA-ES-NPs depicted pH-dependent PLB release characteristics. All nanoformulations exhibited rapid PLB release properties at pH 4.5. This rapid release can be attributed to the protonation of the CS amino moiety, which enhances

the dissolution of the amino group in water and facilitates faster PLB release. Conversely, at pH 7.4, the protonation of CS was less pronounced, resulting in a compact NPs structure and gradual drug diffusion. In both pH media, free PLB was released more rapidly due to the dialysis membrane acting as a regulatory barrier. The initial burst release from the NPs continued for up to 2 h, likely due to drug release from the surface and the quicker diffusion of the drug near the surface of the NPs. Subsequently, slower drug diffusion from the NPs core and inner regions contributed to sustained PLB release. PLB is distributed throughout the polymer matrix of the NPs, which may necessitate more time for the drug to access the NPs surface. Moreover, the release pattern at pH 6.5 has faster than at 7.4 pH but slower than at 4.5 pH. Additionally, pH 4.5 (rapid release) can be advantageous for cancer treatment, given the acidic environment typically associated with tumors [129].

4.5.3.2 Hemolysis and hemocompatibility study

4.5.3.2.1 Blood Smear

Nanomaterials fall within the size range of viruses, and immune-stimulating antigens have the potential to enhance the body's immune responses, induce inflammation, and influence hematological parameters [130]. To assess the potential toxicities of PLB, UMN, PLB-UMN-CS-NPs, PLB-UMN-CS-FA-NPs, PLB-UMN-CS-ES-NPs, and PLB-UMN-CS-FA-ES-NPs, we conducted hematological testing. In this research, deionized water, which induces 100% hemolysis, served as a positive control, while normal saline was used as a negative control (nonhemolytic). Blood samples were subjected to various formulation treatments and then incubated with Leishman stain to examine through a bright microscope (**Figure. 4.4A**). The collected images revealed that the shape and size of the blood cells were not significantly altered by exposure to PLB, UMN, PLB-UMN-CS-NPs, PLB-UMN-CS-FA-NPs, PLB-UMN-CS-ES-NPs, or PLB-UMN-CS-FA-ES-NPs, and were comparable to the saline-treated samples.

4.5.3.2.2 Hemolytic assay

Analyzing the percentage of hemolysis that happened after incubation with various nanoformulations enabled researchers to assess the hematological toxicity of PLB, UMN, PLB-UMN-CS-NPs, PLB-UMN-CS-FA-NPs, PLB-UMN-CS-ES-NPs, and PLB-UMN-CS-FA-ES-NPs. Hemolysis % of PLB, UMN, PLB-UMN-CS-NPs, PLB-UMN-CS-FA-NPs, PLB-UMN-CS-ES-NPs and PLB-UMN-CS-FA-ES-NPs were 2.825 ± 0.08 %, 1.813 ± 0.04 %, 1.201± 0.12 %, 1.310 ± 0.09, 1.152± 0.12 % and 1.382±0.10 %, respectively. The results indicated that PLB, UMN, PLB-UMN-CS-NPs, PLB-UMN-CS-FA-NPs, PLB-UMN-CS-ES-NPs, and PLB-UMN-CS-FA-ES-NPs did not cause hemolysis in human blood (**Figure 4.4B**).

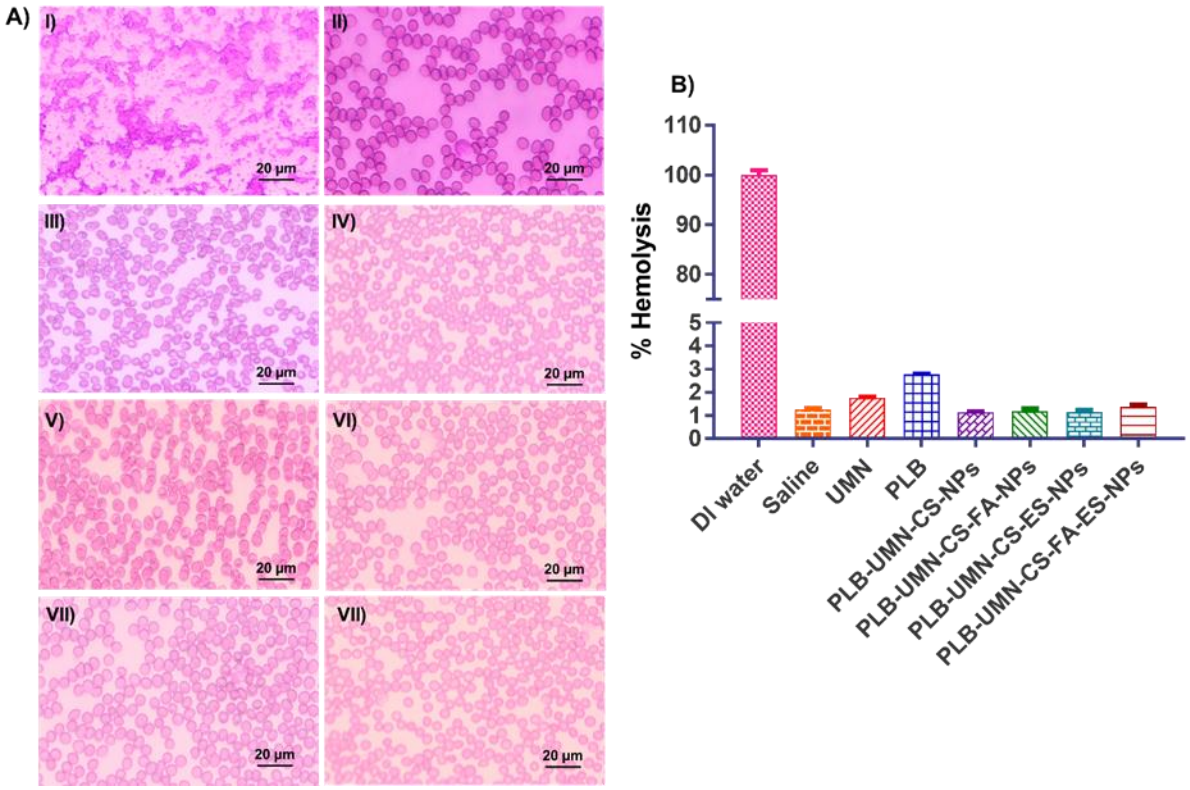

Figure 4.4 (A) Hemocompatibility study; I) DI water, II) Saline, III) UMN, IV) PLB, V) PLB-UMN-CS-NPs, VI) PLB-UMN-CS-FA-NPs, VII) PLB-UMN-CS-ES-NPs and VIII) PLB-UMN-CS-FA-ES-NPs, (B) Hemolysis study; DI water, Saline, UMN, PLB, PLB-UMN-CS-NPs, PLB-UMN-CS-FA-NPs, PLB-UMN-CS-ES-NPs and PLB-UMN-CS-FA-ES-NPs,

4.5.3.3 *In vitro* physiological stability

The PS, ZP, and EE data of the NPs before and after incubation in plasma and serum demonstrated the developed NPs were stable (**Figure. 4.5**). The variation in the PS, ZP, and EE before and after incubation did not show any significant changes (P> 0.05).

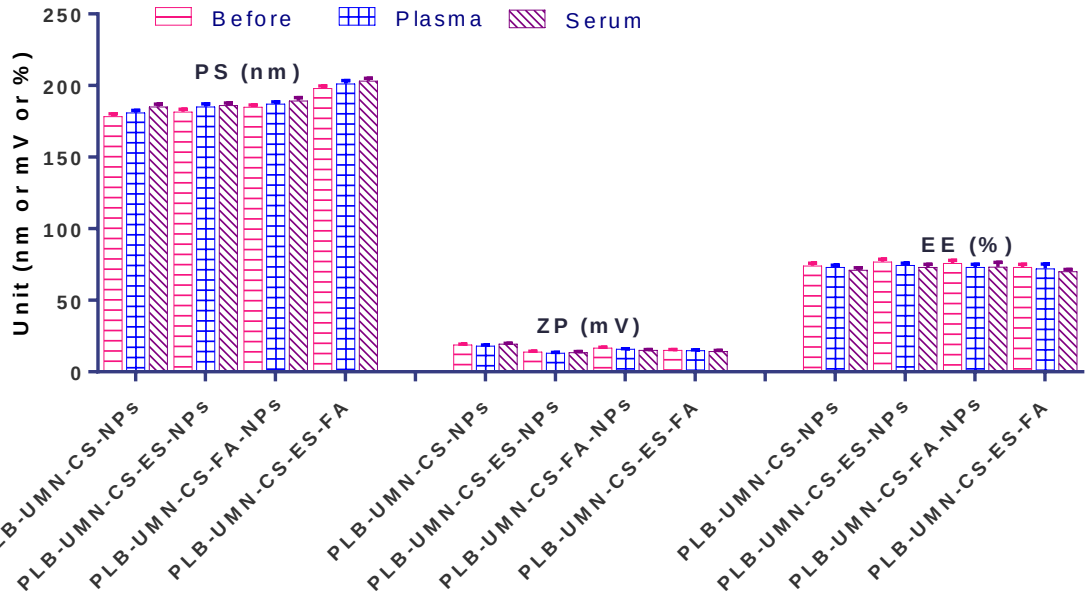

Figure 4.5 *In vitro* physiological stability of the NPs in plasma and serum.

4.5.3.4 *In vitro* cellular uptake study

A critical factor in predicting or assessing the therapeutic effectiveness of NPs is the cellular uptake of the developed NPs. In this current research, an active targeted drug delivery approach based on receptors was employed to enhance the cellular uptake of NPs in breast tumors that are both ER and FR. The incubation of the UMN, PLB-UMN-CS-NPs, PLB-UMN-CS-FA-NPs, PLB-UMN-CS-ES-NPs, and PLB-UMN-CS-FA-ES-NPs with MCF-7 cells and T-47D cells at 20 µg/ml of UMN depicted that PLB-UMN-CS-NPs, PLB-UMN-CS-FA-NPs, PLB-UMN-CS-ES-NPs, and PLB-UMN-CS-FA-ES-NPs had increased cellular localization relative to the free UMN **(Figure 4.6)**. Furthermore, compared to nontargeted NPs, both FR-targeted and ER-targeted, as well as dual-targeted NPs, showed significantly increased fluorescence. This suggests that the cellular

localization of ES and/or FA-conjugated targeted NPs occurs through receptor-mediated cellular uptake. MCF-7 cells and T-47D cells have upregulated membrane estrogen receptors (mER) [132, 133].

Nontargeted NPs were taken up by cells through passive diffusion, involving the adherence of the nanoformulation to cancerous cells and its subsequent passive uptake into the cells. This passive uptake is facilitated by the leaky nature of blood vessels supplying the tumor, leading to increased penetration and retention effects by nontargeted NPs. Nontargeted nanoformulation was taken up by MCF-7 and T-47D cells (**Figure 4.6A and B**). In contrast, targeted nanoformulation demonstrated improved cellular uptake due to ER and FR expression. Additionally, receptor inhibition with free ES and FA decreased cellular internalization of PLB-UMN-CS-FA-ES-NPs, confirming ER/FR-mediated cellular internalization of NPs in MCF-7 and T-47D cells. Following the cellular uptake of UMN, PLB-UMN-CS-NPs, PLB-UMN-CS-FA-NPs, PLB-UMN-CS-ES-NPs, and PLB-UMN-CS-FA-ES-NPs, the percentage mean fluorescent intensity (green and blue channel) per cell in MCF-7 cells and T-47D cells was calculated using ImageJ software (**Figure 4.6 C and D**).

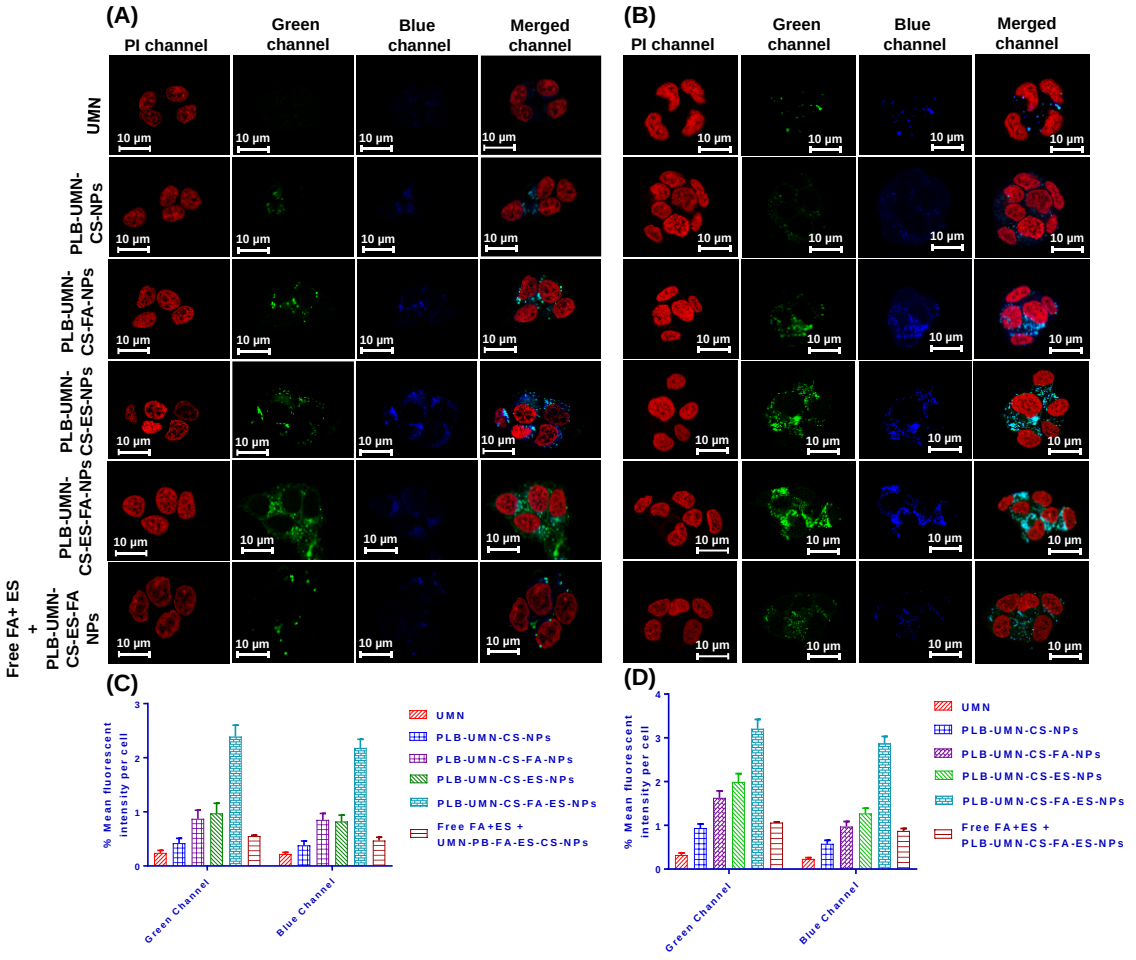

Figure 4.6 Cellular uptake of the free UMN, PLB-UMN-CS-NPs, PLB-UMN-CS-FA-NPs, PLB-UMN-CS-ES-NPs, PLB-UMN-CS-FA-ES-NPs and after pretreatment with FA+ ES in (A) MCF-7 cells and (B) T-47D cells. % Mean fluorescent intensity per cell in (C) MCF-7 cells and (D) T-47D cell following cellular internalization of PLB-UMN-CS-NPs, PLB-UMN-CS-FA-NPs, PLB-UMN-CS-ES-NPs and PLB-UMN-CS-FA-ES-NPs.

4.5.3.5 *In vitro* cytotoxicity assay

Based on the findings, pure PLB does not significantly affect cell viability at lower concentrations. However, its efficacy in MCF-7 cells increased by approximately 9.79-fold when it was entrapped within nontargeted NPs. Furthermore, it was observed that receptor-mediated drug delivery using NPs was more efficient than passive drug delivery.

Pure PLB exhibited IC_{50} at ~40.63 µg/ml, while PLB-UMN-CS-NPs, PLB-UMN-CS-FA-NPs, PLB-UMN-CS-ES-NPs and PLB-UMN-CS-FA-ES-NPs were found at ~4.15 µg/ml, ~1.29 µg/ml, ~1.56 µg/ml, and ~0.75 µg/ml respectively. **(Figure 4.7 A & B)**. In T-47D cells, the IC_{50} of PLB was observed at ~48.15 µg/ml, while IC_{50} of PLB-UMN-CS-NPs,

PLB-UMN-CS-FA-NPs, PLB-UMN-CS-ES-NPs, and PLB-UMN-CS-FA-ES-NPs were observed at ~5.92 µg/ml, 1.65 µg/ml, 2.07 µg/ml, 1.14 µg/ml **(Figure 4.7 C & D)**. The obtained IC_{50} value of the pure PLB was in good agreement with data reported in the literature [149]. The presence of the receptor-targeting group in the developed nanoformulation significantly enhances the efficacy of PLB, making it approximately 57 times more effective for cancer treatment. This substantial improvement is attributed to the overexpression of ER in MCF-7 and T-47D cells, which allows receptor-mediated targeted administration of PLB to enhance its anti-tumor effectiveness significantly. Furthermore, it was observed that blank NPs had no significant cytotoxic effects on MCF-7 and T-47D cells, with cellular viabilities exceeding 95% and 96%, respectively. This demonstrates that blank nanoformulations were nontoxic to MCF-7 and T-47D cells.

In a recent study by Parsian *et al.,* magnetic dendrimers entrapped with PLB were designed, and the researchers investigated the impact on cell viability in various mammary carcinoma cell lines. They found that PLB-encapsulated magnetic dendrimers exhibited higher cytotoxicity against MCF-7 cells compared to MDA-MB-231 cells and SKBR3 cells. In MCF-7 cells, they observed up to a 30% reduction in cell viability [150].

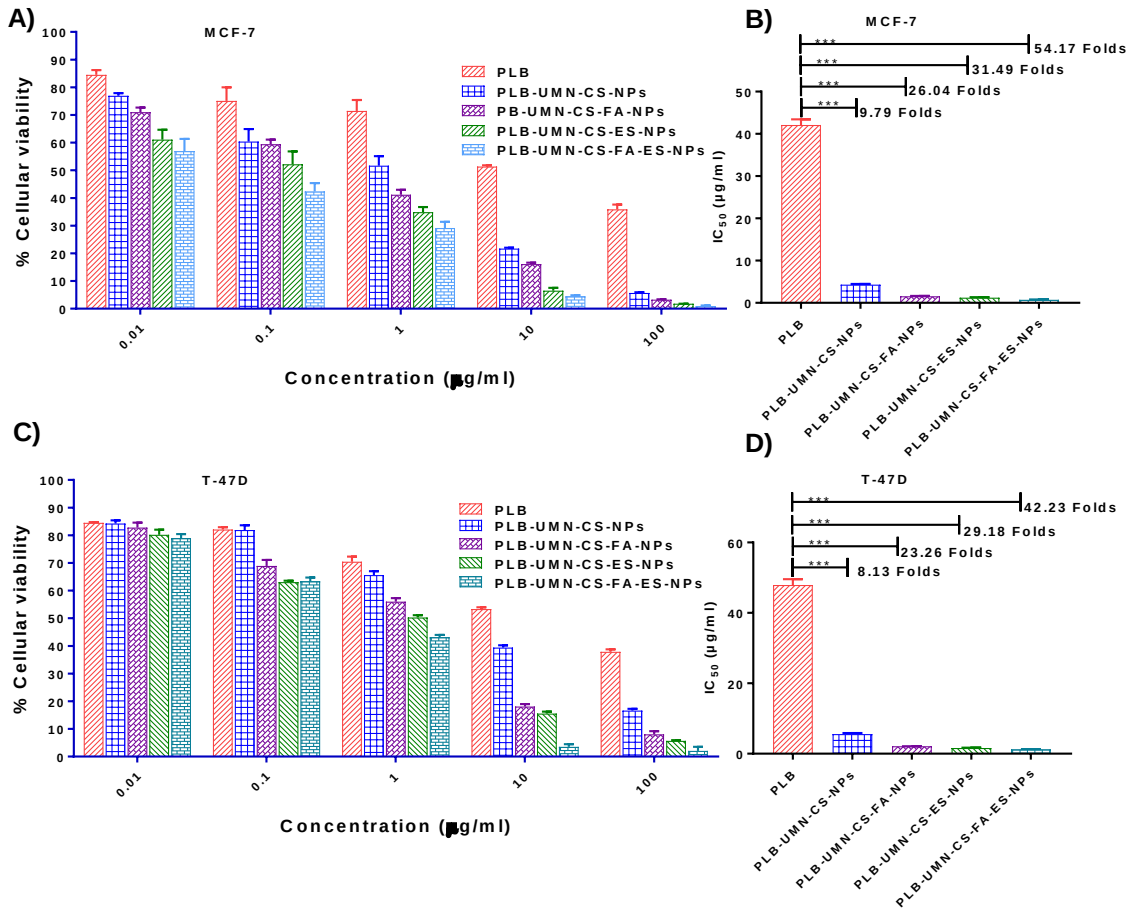

Figure 4.7 Cellular cytotoxicity assessment of the PLB, PLB-UMN-CS-NPs, PLB-UMN-CS-FA-NPs, PLB-UMN-CS-ES-NPs, and PLB-UMN-CS-FA-ES-NPs on MCF-7 cells (A & B) and T-47D cells (C & D).

4.5.3.6 Cell cycle analysis

The use of flow cytometry analysis has confirmed the mechanism through which both the PLB and PLB-loaded NPs reduce the proliferation of MCF-7 cells. PLB works as a CDK4/6 reversible inhibitor. It functions by inhibiting retinoblastoma (Rb) phosphorylation, which thus prevents the growth of the cell cycle from the G1 phase to the S phase. After treating MCF-7 cells with PLB, PLB-UMN-CS-NPs, PLB-UMN-CS-FA-NPs, PLB-UMN-CS-ES-NPs, and PLB-UMN-CS-FA-ES-NPs, the cells were stained with PI and analyzed using a flow cytometer. The collected data were analyzed using Cytoflex software. The prepared formulations, PLB-UMN-CS-NPs, PLB-UMN-CS-FA-NPs, PLB-UMN-CS-ES-NPs, and PLB-UMN-CS-FA-ES-NPs, have significantly improved cell cycle

arrest in the G1 phase, with increases of approximately 1.11-fold, 1.27-fold, 1.33-fold and 1.60-fold increases, respectively, relative to pure PLB (**Figure 4.8**). Cellular uptake and the MTT test results were in good agreement with the results of the cell cycle study.

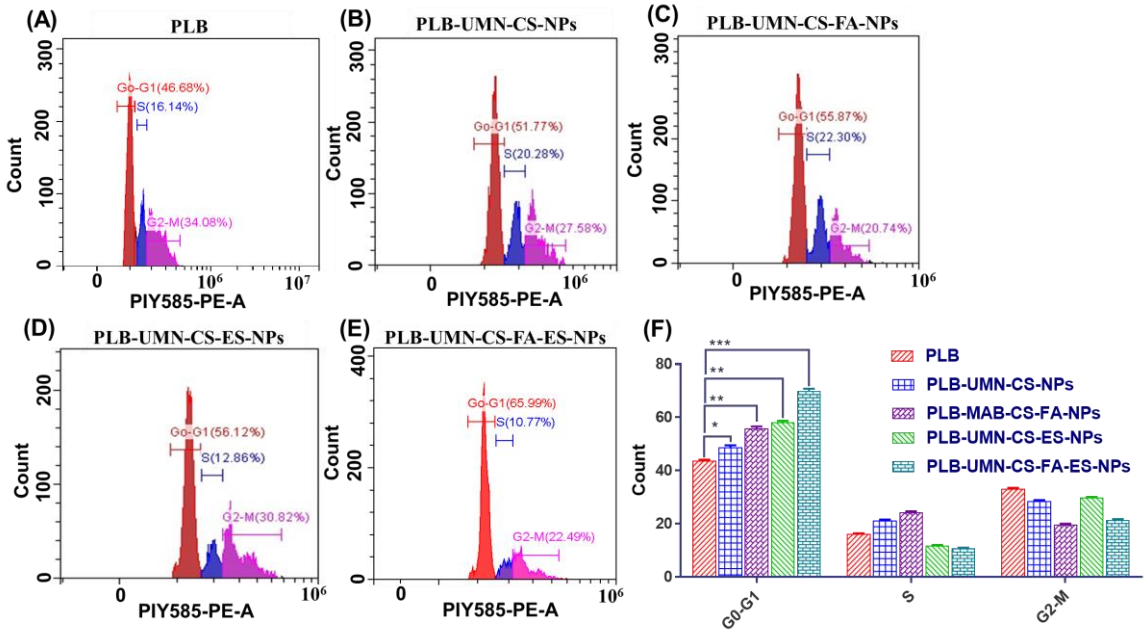

Figure 4.8 Cell cycle study of MCF-7 cells following incubation with A) free PLB, B) PLB-UMN-CS-NPs, C) PLB-UMN-CS-FA-NPs, D) PLB-UMN-CS-ES-NPs and E) PLB-UMN-CS-FA-ES-NPs, F) Graphical presentation of cell cycle study of free PLB, PLB-UMN-CS-NPs, PLB-UMN-CS-FA-NPs, PLB-UMN-CS-FA-ES-NPs.

4.5.4 Pharmacokinetic study

Free PLB, PLB-UMN-CS-NPs, PLB-UMN-CS-FA-NPs, PLB-UMN-CS-ES-NPs, and PLB-UMN-CS-FA-ES-NPs formulations were administered at a dose of 5.91 mg/kg and concentration of the PLB in the plasma (ng/ml) was estimated and are plotted the graph against time (h), (**Figure 4.9**). Additionally, using the obtained data, various pharmacokinetic parameters (Table 4.3) were calculated using Kinetica® 5.0. The bioavailability of PLB-UMN-CS-NPs, PLB-UMN-CS-FA-NPs, PLB-UMN-CS-ES-NPs, and PLB-UMN-CS-FA-ES-NPs has exhibited substantial enhancements, with increases of 3.51, 5.05, 4.23, and 5.58-fold, respectively, in comparison with free PLB. Additionally, the half-life ($T_{1/2}$) has been extended by 1.70, 1.76, 1.84, and 2.00-fold, respectively, in

these formulations. Overall, loading PLB within NPs has significantly enhanced the drug's pharmacokinetic characteristics.

Table 4.3 Pharmacokinetic parameters of PLB, nontargeted NPs, folate receptor targeted NPs, estrogen receptor targeted NPs and dual receptor targeted NPs after *i.v* injection at an equivalent PLB dose of 5.91 mg/kg.

Parameters	**PLB (Mean ± SD*)**	**PLB-UMN-CS-NPs (Mean ± SD*)**	**PLB-UMN-CS-FA-NPs (Mean ± SD*)**	**PLB-UMN-CS-ES-NPs (Mean ± SD*)**	**PLB-UMN-CS-FA-ES-NPs (Mean ± SD*)**
AUC_{total} (ng.h/ml)	23711.86 ± 1458.78	83268.13 ± 1632.72	93613.36 ± 1841.35	88457.41 ± 1739.25	102425.48 ± 2136.45
C_{max} (ng/ml)	6048.69 ± 132.85	5901.13 ± 71.54	6298.21 ± 87.42	6203.12 ± 42.82	6432.21 ± 56.72
$T_{1/2}$ (h)	17.78 ± 1.03	30.37 ± 2.21	31.98 ± 3.02	31.48 ± 2.95	33.11 ± 2.88
MRT (h)	14.87 ± 0.89	35.70 ± 1.62	38.02 ± 1.89	37.19 ± 2.10	40.36 ± 1.93
V_d (l/kg)	1.28 ± 0.04	0.62 ± 0.01	0.58 ± 0.03	0.60 ± 0.02	0.55 ± 0.03
Cl_{total} (ml/kg. h)	49.84 ± 0.73	14.19 ± 0.81	12.63 ± 0.87	13.36 ± 0.42	11.54 ± 0.24
K_E (h^{-1})	0.038 ± 0.004	0.023 ± 0.002	0.022±0.001	0.022 ± 0.003	0.021±0.002
F_R	-	3.51	3.95	3.73	4.32

*n = 3; S.D: Standard deviation
Blank CS NPs: Blank chitosan nanoparticles
PLB-UMN-CS NPs: Non-targeted theranostic nanoparticles
PLB-UMN-CS-ES NPs: Estrogen receptor targeted theranostic nanoparticles
PLB-UMN-CS-FA NPs: Folate receptor targeted theranostic nanoparticles
PLB-UMN-CS-ES-FA NPs: Estrogen receptor and folate receptor targeted theranostic nanoparticles

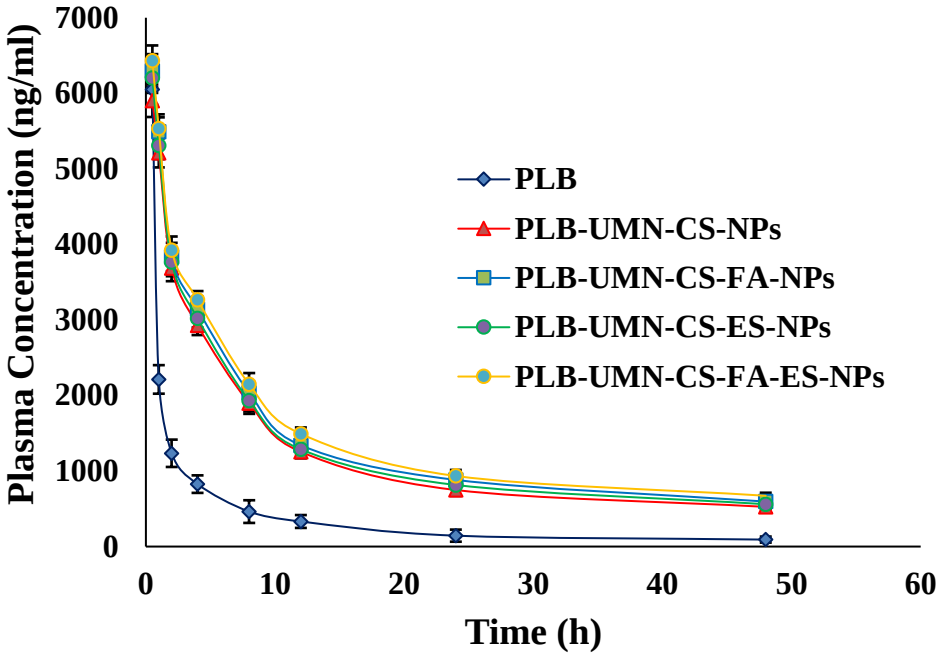

Figure 4.9 Pharmacokinetic study of PLB, PLB-UMN-CS-NPs, PLB-UMN-CS-FA-NPs, PLB UMN-CS-ES-NPs and PLB-UMN-CS-FA-ES-NPs following *i.v.* injection.

4.5.5 Histopathology Study

After administering free PLB and various nanoparticle formulations (PLB-UMN-CS-NPs, PLB-UMN-CS-FA-NPs, PLB-UMN-CS-ES-NPs, and PLB-UMN-CS-FA-ES-NPs) at a dose of 5.91 mg/kg, collected organs were processed and stained with H & E stain. H & E staining is used in histology to differentiate tissue components, with hematoxylin staining nuclei blue or purple and eosin staining cytoplasm and extracellular matrix pink or red. This technique enables detailed visualization of tissue structure and composition for examination and diagnosis. The organs were examined under a microscope, and images were acquired and represented in **Figure 4.10.** The H & E stained images of the healthy rats were analyzed, and comparisons were done with rats treated with nanoformulation to evaluate any potential toxicity arising from the administration of various formulations. A comprehensive analysis of the H & E images from healthy rats

showed the absence of pathological lesions in their vital organs. Conversely, animals administered with free PLB displayed pathological in vital organs, which is indicated by black arrow in **Figure 4.10**. The histopathological investigations indicate that nontargeted NPs have led to a relatively enhanced safety PLB treatment. Further, the administration of PLB-UMN-CS-FA-NPs, PLB-UMN-CS-ES-NPs, and PLB-UMN-CS-FA-ES-NPs have not exhibited any visible toxic effects on the organs, and the resulting images closely resembled those of the healthy rats [103].

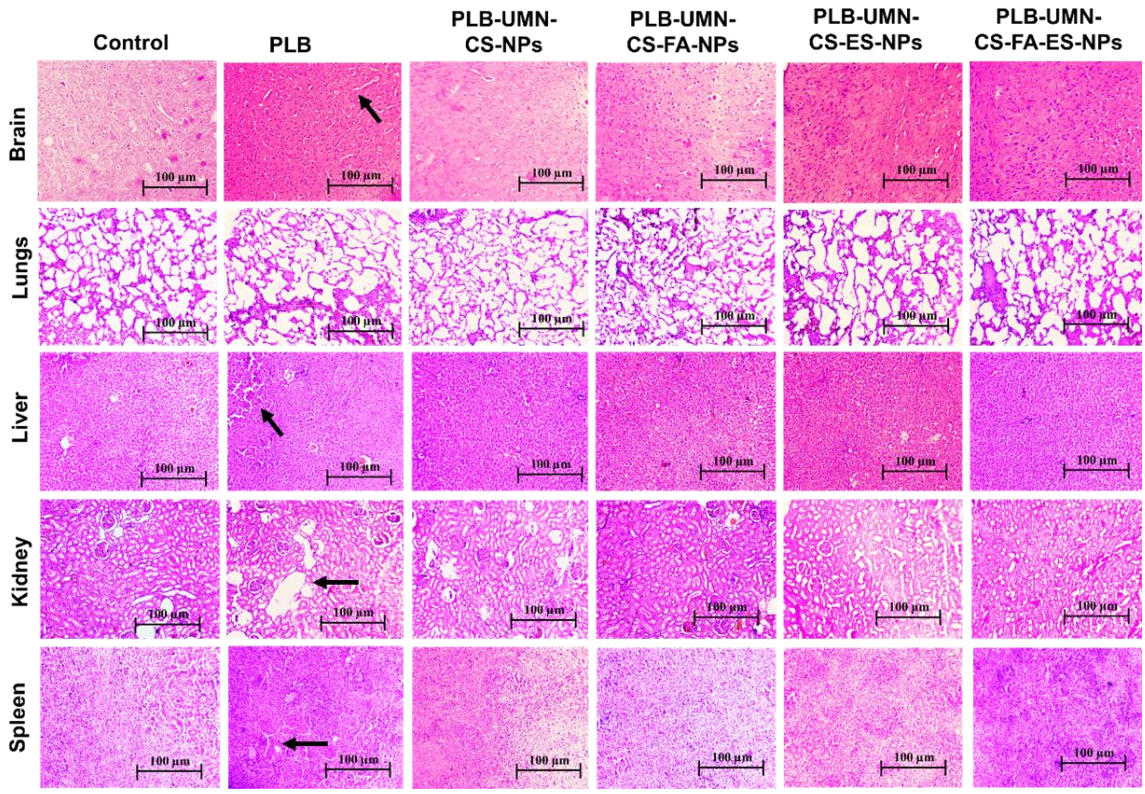

Figure 4.10. H & E stained images following administration with PLB, PLB, PLB-UMN-CS-NPs, PLB-UMN-CS-FA-NPs, PLB-UMN-CS-ES-NPs and PLB-UMN-CS-FA-ES-NPs**.** The arrow in black color indicated lesion/damage to vital organs.

4.5.6 *In vivo* breast tumor imaging by USG/PA

This study involved the examination of SD rats with breast tumors by utilizing photoacoustic and ultrasound imaging techniques. The imaging was conducted prior to the initiation of any treatments and afterward on the 2nd, 4th, and 6th days post-treatment. The breast tumor's ultrasound and photoacoustic pictures exhibited a notable decrease in tumor

size after the injection of targeted theranostic nanoformulation, as compared to nontargeted theranostic nanoformulation and free PLB. Additionally, the control group exhibited an increase in tumor size, comprising animals who were solely administered saline without any form of treatment. On the 6th day of the study, it was observed that the breast tumor had totally disappeared in animals that received the dual-targeted NPs, as depicted in **Figure 4.11A and B**.

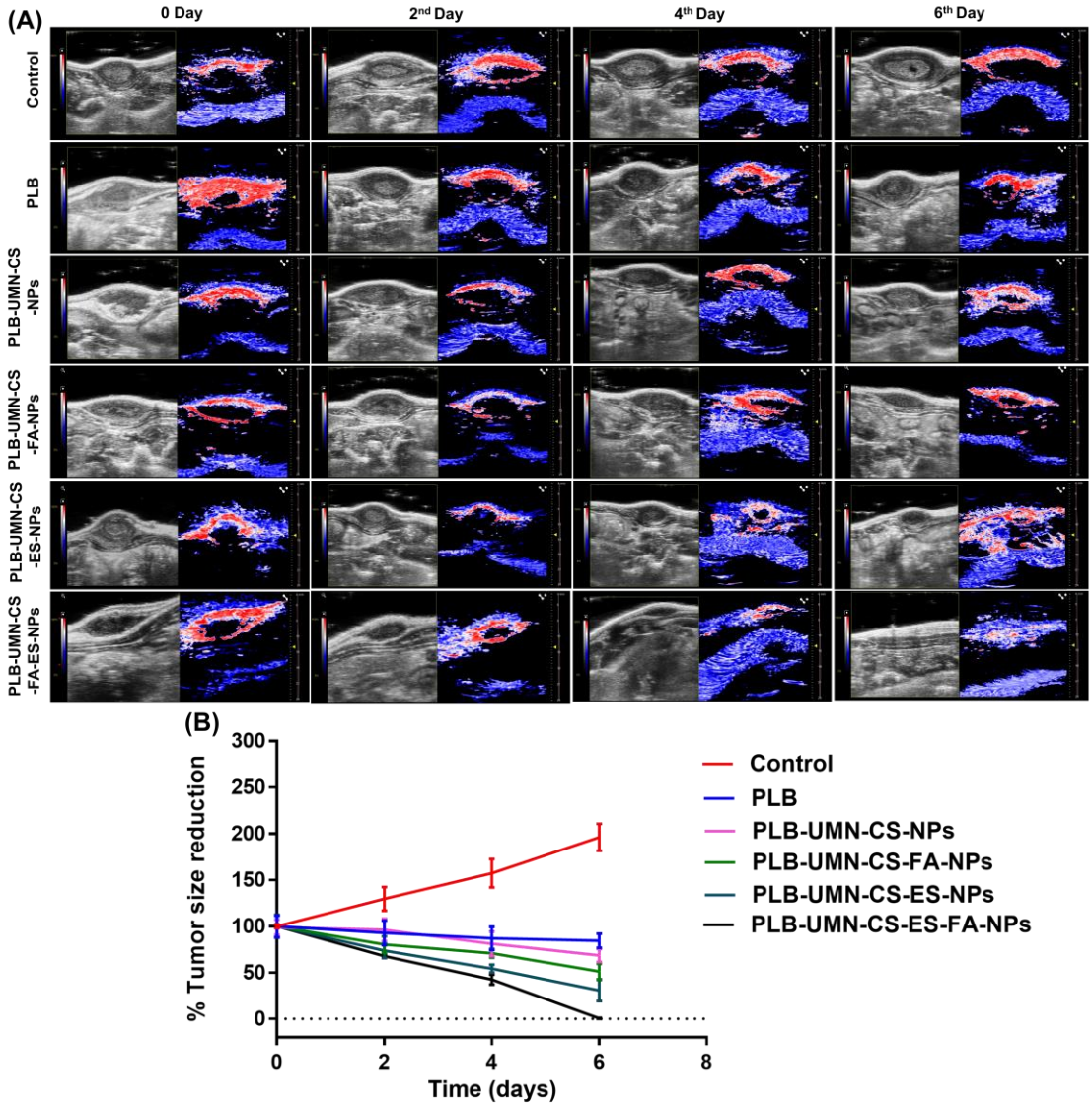

Figure 4.11 (A) *In vivo* breast tumor imaging of the rat by USG and PA imaging before and after treatment with PLB, PLB-UMN-CS-NPs, PLB-UMN-CS-FA-NPs, PLB-UMN-CS-ES-NPs and PLB-UMN-CS-FA-ES-NPs, (B) Comparison of breast tumor size reduction among control, PLB, PLB-UMN-CS-NPs, PLB-UMN-CS-FA-NPs, PLB-UMN-CS-ES-NPs, and PLB-UMN-CS-FA-ES-NPs treated groups.

Tissue hypoxia is characterized by an insufficient supply of oxygen to a particular tissue, which may hinder its biological functions. Hypoxia is a well-recognized characteristic of solid malignant tumors and occurs when the oxygen supply becomes inadequate at a distance greater than 70 to 150 μm from the tumor's vascular system. This condition is caused by the rapid proliferation of malignant cells, which outpaces the development of the tumor's blood vessels, resulting in oxygen depletion in the surrounding tissue [151, 152].

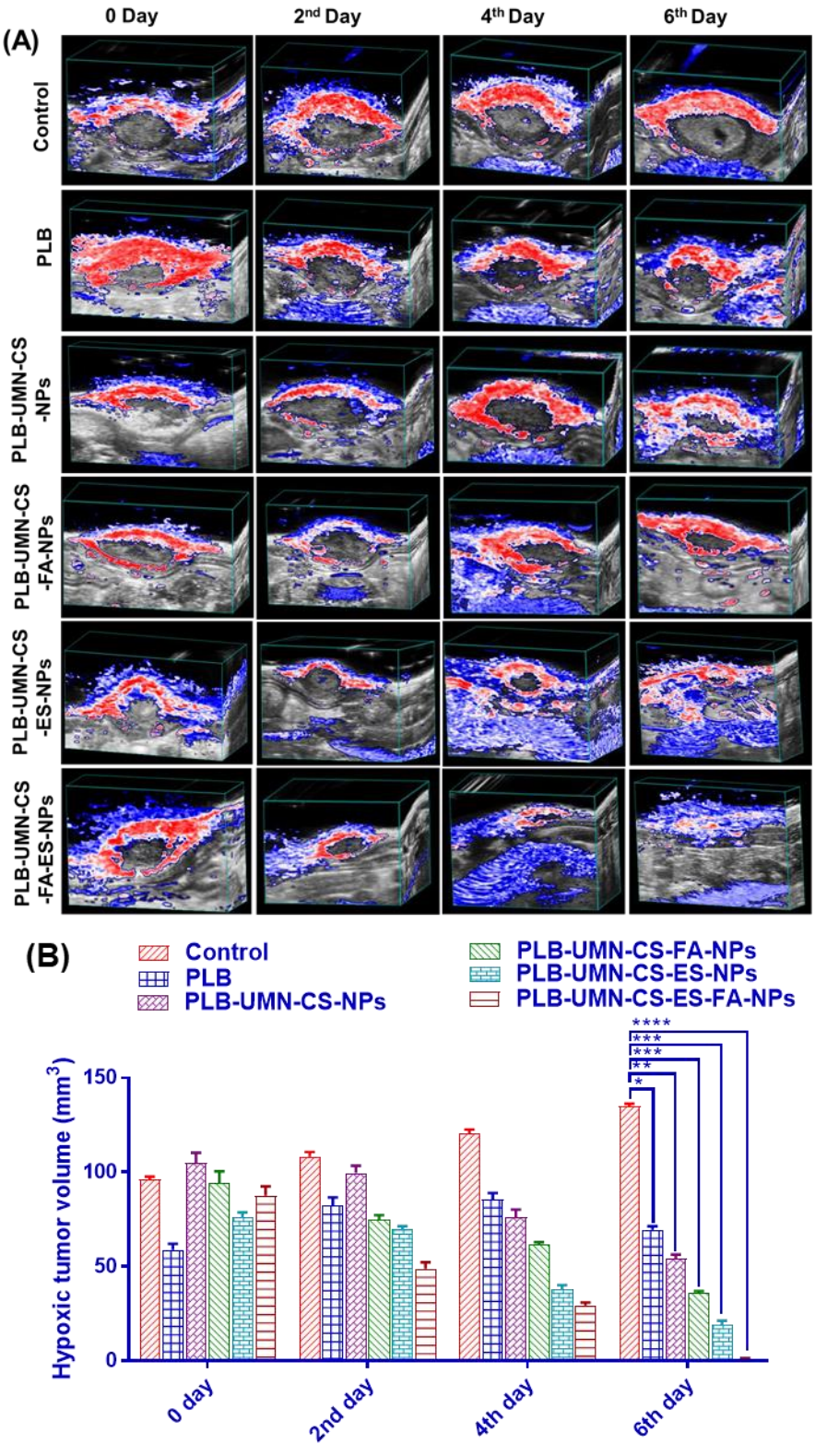

Figure 4.12 (A) Hypoxic breast tumor volume estimation in rats by USG and PA imaging following administration with PLB, PLB-UMN-CS-NPs, PLB-UMN-CS-FA-NPs, PLB-UMN-CS-ES-NPs and PLB-UMN-CS-FA-ES-NPs and (B) Statistical comparison of the hypoxic tumor volume among different treatment groups.

Experimental and clinical research have shown that hypoxia is crucial to solid tumors. The pathophysiology of malignant tumors disrupts tumor microcirculation. These abnormalities worsen oxygen diffusion, causing tumor hypoxia [153]. Intratumoral hypoxia, caused by vascular endothelium functional and structural abnormalities, is often associated with a more malignant phenotype, metastasis, and treatment resistance [136]. Tumors that possess similar size and structural properties might display variable levels of hypoxia and vascularization. Before initiating the study, it was ensured that all groups of rats with breast tumors had comparable levels of hypoxic tumor volume and tumor vascularization, as represented in **Figure 4.12.** Following the treatment interventions, a significant reduction ($P < 0.05$) in hypoxic tumor volume was observed in the group treated with NPs. Specifically, by the 6th day after dual-targeted NPs treatment, hypoxic tumor volume had completely disappeared (**Figure 4.12A & 7B**). However, on 6^{th} day free PLB, PLB-UMN-CS-NPs, PLB-UMN-CS-FA-NPs and PLB-UMN-CS-ES-NPs treated rats had 69.47 ± 1.89, 54.11±2.24, 35.77±1.24, 19.37±1.98 mm^3 hypoxic tumor volume, respectively. It was observed that on 6^{th} day, the control group of rats had a hypoxic tumor volume of 134.95±1.27 mm^3, which is significantly higher than the hypoxic tumor volume (96.20±1.38 mm^3) on 0 days.

Tumor growth necessitates a continuous and heightened provision of nutrients to sustain the tumor cells, thereby stimulating the formation of blood vessels (angiogenesis) both within and around the tumor. Vasculature development was arrested and progressively diminished over time, ultimately ceasing entirely by the 6th day of treatment in the rats that received dual-targeted NPs, as illustrated in **Figure 4.13A & B**. The % vascularity on the 6^{th} day in the breast tumor of the rats after treatment with free PLB, PLB-UMN-CS-NPs, PLB-UMN-CS-FA-NPs, and PLB-UMN-CS-ES-NPs were 2.28±0.18, 1.76±0.10, 1.36±0.12, 0.51±0.08, and 0.06±0.01 %, respectively. In contrast, the group receiving ER-

targeted NPs and FR-targeted NPs treatment exhibited a significant decline in tumor vascularity up to the 6^{th} day relative to the nontargeted and free PLB group. Additionally, nontargeted NP and free PLB treated rats show a slight decrease in tumor vascularity, whereas the control group depicted an increase in tumor vascularity (8.12±0.60 %) over time.

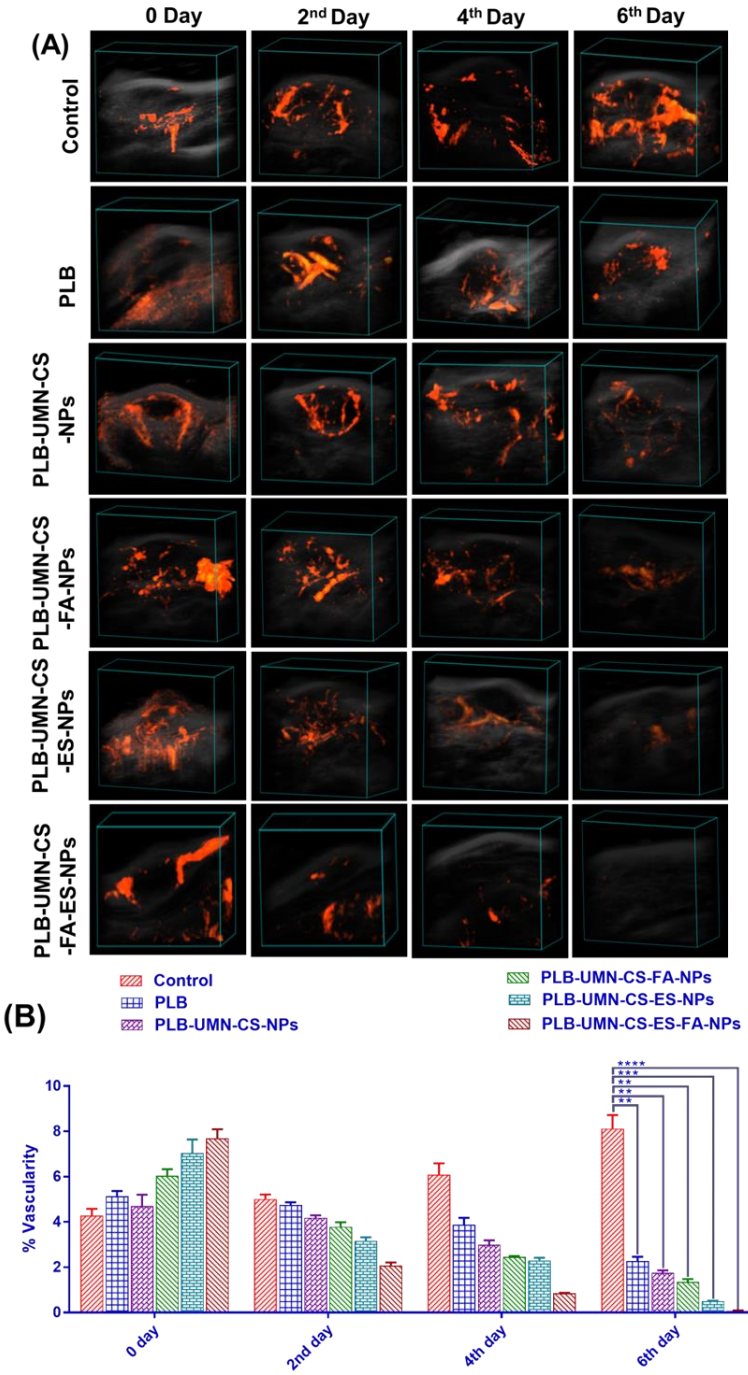

Figure 4.13 (A) Breast tumor images showing tumor vascularity following treatment with PLB, PLB-UMN-CS-NPs, PLB-UMN-CS-FA-NPs, PLB-UMN-CS-ES-NPs and PLB-UMN-CS-FA-ES-NPs and (B) Statistical comparison of tumor vascularity among different treatment group.

Furthermore, after six days, tumor samples from the six groups of animals that were mentioned were removed and subsequently underwent H & E staining. The pictures were acquired utilizing a bright microscope at a magnification of 400X. **Figure 4.14A** illustrates the healthy rat breast (normal animal, without tumor), while the saline treated group

(consisting of breast tumor rats) received saline and displayed tumor growth in the breast lobes, which was characterized by the presence of aberrant small and big nuclei. The nuclei in each image were counted by processing H&E images into black and white (B & W) by using Image J software, as shown in **Figure 4.14B**.

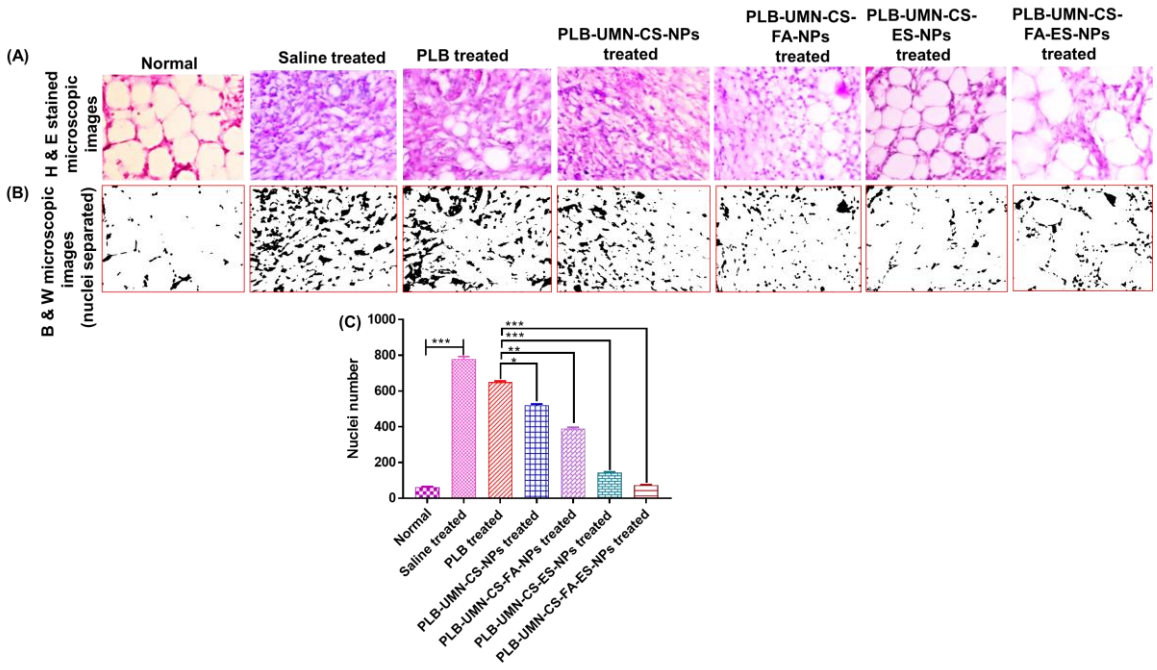

Figure 4.14 A) Histopathological H & E staining of normal, saline treated, PLB, PLB-UMN-CS-NPs, PLB-UMN-CS-FA-NPs, PLB-UMN-CS-ES-NPs and PLB-UMN-CS-FA-ES-NPs treated rat breast tumor samples. B) B&W images of separated nuclei of normal, saline treated, PLB, PLB-UMN-CS-NPs.

The number of nuclei observed in normal, saline treated, PLB, PLB-UMN-CS-NPs, PLB-UMN-CS-FA-NPs, PLB-UMN-CS-ES-NPs and PLB-UMN-CS-FA-ES-NPs treated group were 62 ± 4.45, 780 ± 12.75, 650 ± 6.98, 520 ± 7.75, 390 ± 6.8, 143 ± 4.54 and 73 ± 3.15, respectively (**Figure 4.14C**). The isolated nuclei of the animal groups that received saline treatment numbered 62 ± 4.45, whereas the isolated nuclei of the animals treated with DMBA totaled 780 ± 12.75 ($p < 0.0001$). An increase in the nuclei area suggests the presence of breast tumor growth. Following six days of treatment with free PLB, the tumor does not exhibit many significant effects. However, animals treated with NPs formulation have demonstrated a significant reduction in the tumor cells, and the targeted NPs treated

group after 6th days demonstrated a number of nuclei identical to the healthy animal (**Figure 4.14**). In addition, the tumors in the DMBA-treated rat group were assessed for expression of ER through immunohistochemistry analysis, following the ER scoring guidelines of the College of American Pathologists. This analysis revealed that 2.0 % of the cancer cells exhibited nuclear staining that confirminged the overexpression of ER in DMBA induced breast tumor.

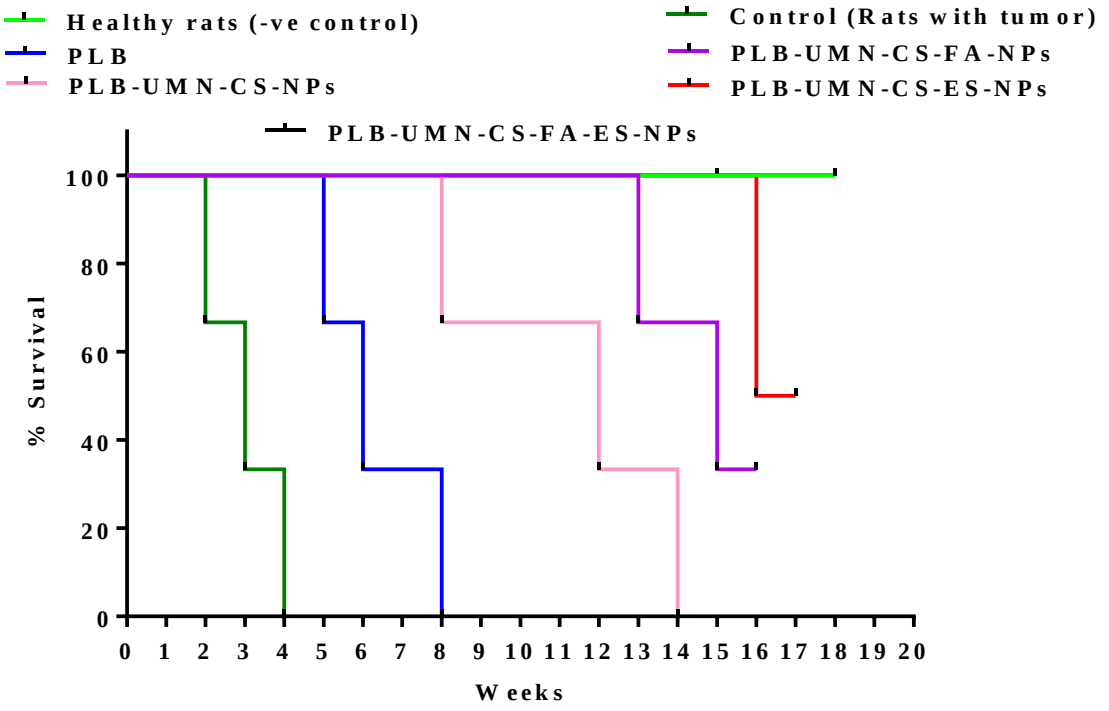

Figure 4.15 Kaplan-Meier survival analysis plot of healthy rats (without tumor), control (rats with tumor, saline treated), PLB, PLB-UMN-CS-NPs, PLB-UMN-CS-FA-NPs, PLB-UMN-CS-ES-NPs, and PLB-UMN-CS-FA-ES-NPs. Healthy rats and PLB-UMN-CS-FA-ES-NPs treated rats had 100 % survival (black and green lines superimposed).

Figure 4.15. represents the post-treatment survival study conducted on rats with DMBA-induced breast tumors. The average survival rate of the animals was determined using Kaplan-Meier survival analysis throughout the 18 weeks. The administration of saline treatment enabled the tumor-bearing control rats to survive for a duration of 4 weeks, whereas the application of PLB treatment extended the survival of the tumor-bearing rats

to 8 weeks. Among the rats that received nontargeted NPs were rats that survived up to 14 weeks. FR-targeted NP and ER-targeted NPs treated rats showed survival of 33.33 % and 66.67%, respectively, in 18 weeks. After 18 weeks, the survival of rats subjected to dual-targeted NPs treatment was comparable to that of normal rats, and both groups of the rats were survived completely beyond 18 weeks.

4.5.7 *In vivo* fluorescent imaging of the breast tumor

The *in vivo* breast tumor images (**Figure 4.16A**) depicted the distribution pattern of free UMN (Control) and prepared formulations, namely PLB-UMN-CS-NPs, PLB-UMN-CS-FA-NPs, PLB-UMN-CS-ES-NPs, and PLB-UMN-CS-FA-ES-NPs, were distributed within 0.5 h after administration across different anatomical regions. However, after 2 h, the targeted NPs began to accumulate specifically in the breast tumor, while the fluorescent signals from free UMN and nontargeted NPs remained low at the tumor site. Additionally, it was seen at the 6 h time point post-administration that the specific NPs being targeted had fully aggregated at the site of the tumor. In contrast, the signals emitted by the free UMN, and nontargeted NPs were rather weak around the tumor area. Furthermore, following a duration of 6 h, it was seen that the concentration of the specific NPs at the site of the tumor began to decrease, maybe as a result of metabolic processes or degradation taking place inside the microenvironment of the tumor. **Figure 4.16B** presents quantitative radiant efficiency signals from free UMN, PLB-UMN-CS-NPs, PLB-UMN-CS-FA-NPs, PLB-UMN-CS-ES-NPs, and PLB-UMN-CS-FA-ES-NPs following administration. The quantitative radiant efficiency signals after 6 h of the administration of the free UMN, PLB-UMN-CS-NPs, PLB-UMN-CS-FA-NPs, PLB-UMN-CS-ES-NPs, and PLB-UMN-CS-FA-ES-NPs in the breast tumor region were found to be $1.87 \times 10^7 \pm 0.4 \times 10^7$, $1.84 \times 10^7 \pm 0.6 \times 10^7$, $36.2 \times 10^7 \pm 5.34 \times 10^7$, $47.1 \times 10^7 \pm 1.75 \times 10^7$ and $51.4 \times 10^7 \pm 3.74 \times 10^7$ ph/sec/cm2/sr, respectively. These findings provide conclusive evidence of the

targeted delivery of PLB-UMN-CS-FA-NPs, PLB-UMN-CS-ES-NPs, and PLB-UMN-CS-FA-ES-NPs to breast tumors.

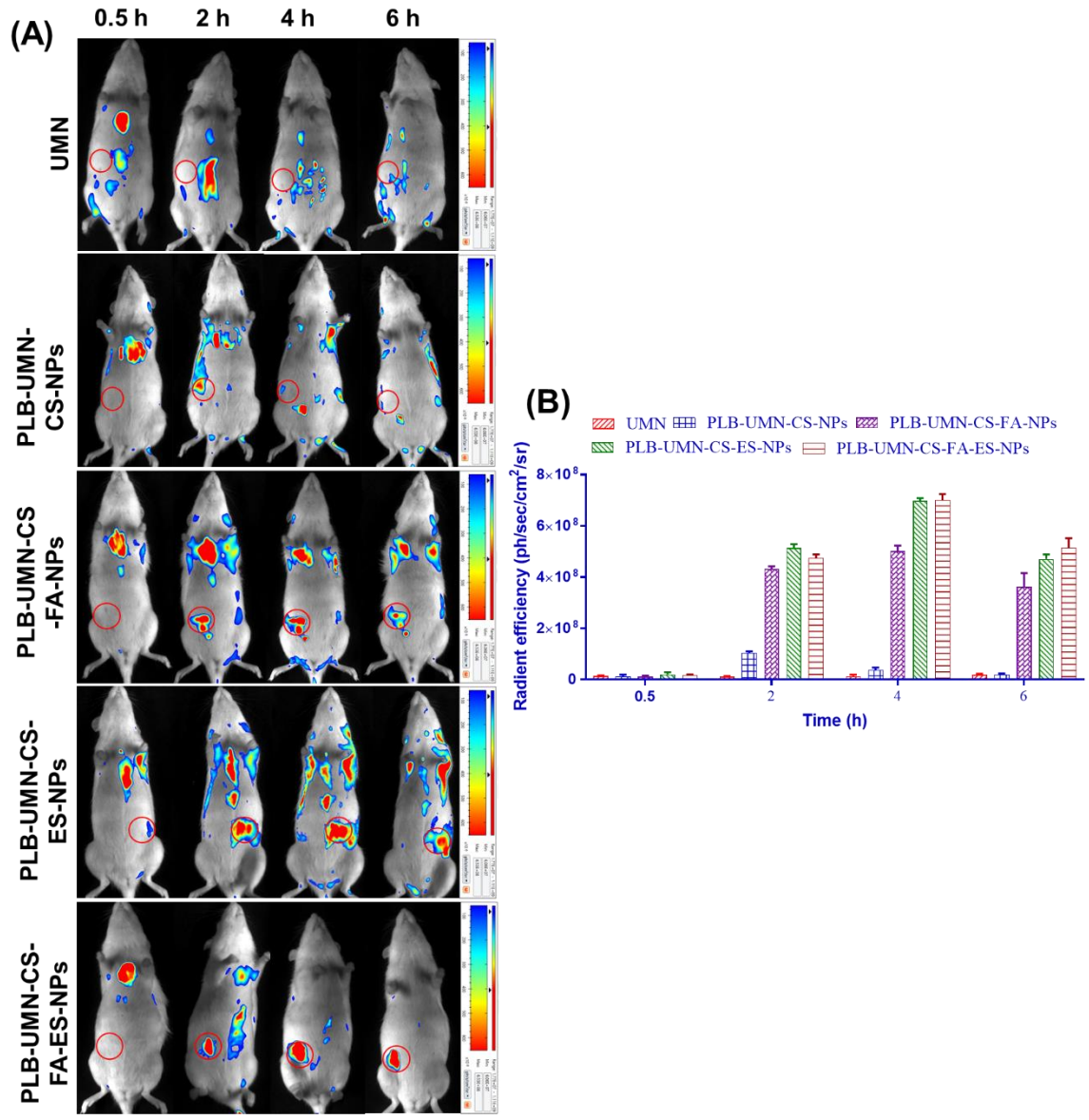

Figure 4.16. Targeted delivery of PLB-UMN-CS-FA-NPs, PLB-UMN-CS-ES-NPs and PLB-UMN-CS-FA-ES-NPs, A) *In vivo* biodistribution of UMN, PLB-UMN-CS-FA-NPs, PLB-UMN-CS-ES-NPs and PLB-UMN-CS-FA-ES-NPs at 0.5, 2, 4 and 6 h after intravenous administration on DMBA induced breast cancer model. B) Histogram showing radiant efficiency of UMN, PLB-UMN-CS-NPs, PLB-UMN-CS-FA-NPs, PLB-UMN-CS-ES-NPs and PLB-UMN-CS-FA-ES-NPs after administration at different time intervals. The breast tumor has been circled (in red) on the left (first, second, third and fifth row) or right (fourth row) side of the breast. ns ($P \geq 0.05$), * ($P < 0.05$), ** ($P < 0.01$), *** ($P < 0.001$), and **** ($P < 0.0001$).

4.6 Conclusion

In conclusion, an ES and FA conjugated CS polymeric theranostic nanoformulation was developed for the targeted imaging and therapy of ER and FR overexpressed breast

tumors. PLB entrapment efficiencies as high as 76.82 % were observed, demonstrating that the ionic gelation and solvent evaporation process was effective in formulating the NPs. Furthermore, NPs were found to be spherical and to have smooth surfaces using FE-SEM, AFM, and TEM investigations. The XPS analysis provided conclusive evidence that ES and or FA was present on the surfaces of NPs and the *in vitro* drug release study demonstrated that NPs possessed a sustained drug release profile. In addition, the analysis of cellular uptake revealed that the targeted NPs accumulated efficiently in MCF-7 cells. Notably, the free ES/FA pretreatment of cells decreased the cellular uptake of the theranostics nanoformulations because of ER and FR blocking, further confirming that receptor-mediated endocytosis is the mechanism underlying the uptake of these targeted NPs. The results of the *in vitro* cytotoxicity assay performed on T-47D and MCF-7 cells demonstrated that the dual-targeted NPs showed notably higher cytotoxicity than free PLB. Specifically, there was a 54.17-fold increase in cytotoxicity observed in MCF-7 cells, while T-47D cells exhibited a 42.23-fold increase in cytotoxicity when exposed to the dual-targeted NPs. The dual-targeted NPs showed a remarkable capability to totally eradicate rat breast tumors in a 6-day period of therapy. This outcome was confirmed by the findings from both ultrasound and photoacoustic imaging techniques. Additionally, the targeted NPs exhibited enhanced effectiveness in decreasing the volume of hypoxic tumors and the presence of blood vessels within the tumors, as compared to nontargeted NPs and free PLB. Moreover, *in vivo* optical imaging in rats demonstrated that dual-targeted theranostic NPs, were significantly accumulated in breast tumors after 6 h of administration compared to the free UMN, nontargeted, FR-targeted, and ER-targeted theranostic NPs.